Available online at www.sciencedirect.com
ScienceDirect
Journal of Computational Physics 227 (2008) 4281–4307
JOURNAL OF COMPUTATIONAL PHYSICS
www.elsevier.com/locate/jcp

On the parametric finite element approximation of evolving hypersurfaces in $\mathbb{R}^3$

John W. Barrett [a,*], Harald Garcke [b], Robert Nürnberg [a]

[a] Department of Mathematics, Imperial College London, London SW7 2AZ, UK
[b] NWF I – Mathematik, Universität Regensburg, 93040 Regensburg, Germany

Received 28 September 2006; accepted 16 November 2007
Available online 29 February 2008

Abstract

We present a variational formulation of motion by minus the Laplacian of curvature and mean curvature flow, as well as related second and fourth order flows of a closed hypersurface in $\mathbb{R}^3$. On introducing a parametric finite element approximation, we prove stability bounds and compare our scheme with existing approaches. The presented scheme has very good properties with respect to the distribution of mesh points and, if applicable, volume conservation.

MSC: 65M60; 65M12; 35K55; 53C44

Keywords: Surface diffusion; (Inverse) mean curvature flow; Surface attachment limited kinetics; Nonlinear surface evolution; Parametric finite elements; Tangential movement

1. Introduction

In this paper we analyze a parametric finite element approximation for the evolution of closed hypersurfaces $\Gamma \subset \mathbb{R}^d$, $d = 3$, moving under given geometric flows such as motion by mean curvature and motion by surface diffusion. The present authors introduced the scheme considered here in [7] for fourth order geometric evolution equations and extended it in various ways, including to the case of second order equations and the presence of external boundaries, in [5]. In both of these papers, only curves and networks of curves in the plane ($d = 2$) were considered. Here we recall, that in this case an intrinsic discrete tangential motion induced by our scheme leads to an almost uniform distribution of nodes along the polygonal approximation of the curve Γ. One aim of this paper will be, to investigate whether this remarkable property extends to surfaces in $\mathbb{R}^3$.

Our approach makes use of a fundamental idea of Dziuk, see [12], who used the identity

$$\Delta_s \vec{x} = \vec{\varkappa} \equiv \varkappa \vec{\nu} \tag{1.1}$$

* Corresponding author.
E-mail addresses: j.barrett@imperial.ac.uk (J.W. Barrett), harald.garcke@mathematik.uni-regensburg.de (H. Garcke), robert.nurnberg@imperial.ac.uk (R. Nürnberg).

0021-9991/$ - see front matter © 2007 Elsevier Inc. All rights reserved.
doi:10.1016/j.jcp.2007.11.023

for the first time in order to design a finite element method for geometric partial differential equations and mean curvature flow; see also [13]. The identity (1.1) is well known from surface geometry, where Δ_s is the surface Laplacian (Laplace–Beltrami operator), $\vec{x}$ is a parameterization of Γ, $\vec{\varkappa}$ is the mean curvature vector with $\varkappa$ the sum of the principal curvatures and $\vec{\nu}$ a unit normal to Γ. Here one uses the sign convention that $\varkappa$ is positive if the surface is curved in the direction of the normal. A second idea stems from [4], where a splitting method and a solver based on a Schur complement approach were proposed in order to compute solutions of the surface diffusion law

$$\mathcal{V} = -\Delta_s \varkappa, \tag{1.2}$$

where $\mathcal{V}$ is the normal velocity of the surface.

The motion of surfaces driven by second or fourth order geometric evolution equations arises in many applications in materials science and in differential geometry. For a closed hypersurface Γ in $\mathbb{R}^d$, which evolves in time, motion by surface diffusion is given by (1.2). The mean curvature flow, on the other hand, is a second order evolution equation and is given by

$$\mathcal{V} = \varkappa. \tag{1.3}$$

In this paper, we are also going to consider more general flows of the form

$$\mathcal{V} = f(\varkappa), \tag{1.4}$$

where $f : (a, b) \to \mathbb{R}$ with $-\infty \leqslant a < b \leqslant \infty$, is a strictly monotonically increasing continuous function, e.g.

$$f(r) := |r|^{\beta-1} r, \quad \beta \in \mathbb{R}_{>0}, \tag{1.5}$$

see [21] and the references therein. For example, in the curve case ($d = 2$), the evolution law (1.4), with (1.5) for $\beta = \frac{1}{3}$, has been studied in [1,25,2]. Of particular interest is the choice

$$f(r) := -r^{-1}, \tag{1.6}$$

i.e. the inverse mean curvature flow, see e.g. [17,20] for the origins of this flow in mathematical physics, where it occurs in the context of the positive mass conjecture; and [19], and the references therein, for a consideration of this flow in differential geometry. Numerical results for the inverse mean curvature flow of surfaces in $\mathbb{R}^3$ have been given in [23], where a finite volume approximation of a regularized level-set formulation of (1.4) with (1.6) is considered. For $d = 3$ we know of no other approach for the approximation of the inverse mean curvature flow in the literature. For parameterizations $\vec{x} : \Omega \times [0, T] \to \mathbb{R}^d$ of Γ, where Ω is a suitable compact reference manifold without boundary in $\mathbb{R}^d$, (1.4) can be written as a second order equation:

$$\mathcal{V} := \vec{x}_t \cdot \vec{\nu} = f(\varkappa), \quad \varkappa \vec{\nu} = \Delta_s \vec{x}. \tag{1.7}$$

Note that because the tangential component $\vec{x}_t - (\vec{x}_t \cdot \vec{\nu})\vec{\nu}$ of the velocity $\vec{x}_t$ is not prescribed in (1.7), there exists a whole family of solutions $\vec{x}$, even though the evolution of Γ is uniquely determined.

A version of (1.4) that preserves the enclosed volume is given by

$$\mathcal{V} = f(\varkappa) - \frac{\int_\Gamma f(\varkappa)\,\mathrm{d}s}{\int_\Gamma 1\,\mathrm{d}s}, \tag{1.8}$$

the so called conserved mean curvature flow, also called surface attachment limited kinetics (SALK), if $f(r) := r$. An intermediate law between (1.4), with $f(r) := r$, and (1.2) is the following evolution law

$$\mathcal{V} = -\Delta_s \left(\frac{1}{\alpha} - \frac{1}{\xi}\Delta_s\right)^{-1} \varkappa, \tag{1.9}$$

where $\alpha, \xi \in \mathbb{R}_{>0}$. The flow (1.9) interpolates between surfaces diffusion (1.2) and SALK, (1.8) with $f(r) := r$, and was first discussed in [28]; see also [14]. It is similar to (1.2) and (1.8) in that the enclosed volume is conserved while the area of the hypersurface decreases. We observe that for $\alpha \to \infty$ and $\xi = 1$, the solutions to (1.9) should converge to solutions of (1.8) with $f(r) := r$, while $\xi \to \infty$ and $\alpha = 1$ corresponds to the law (1.2). The former limit has been rigorously shown in the curve case ($d = 2$), see [15]. Given parameterizations $\vec{x} : \Omega \times [0, T] \to \mathbb{R}^d$ of Γ, (1.9) can be written as a system of second order equations:

$$\vec{x}_t \cdot \vec{\nu} = -\Delta_s y, \quad \left(\frac{1}{\alpha} - \frac{1}{\xi}\Delta_s\right) y = \varkappa, \quad \varkappa\vec{\nu} = \Delta_s \vec{x}. \tag{1.10}$$

Analogously surface diffusion, (1.2), can be rewritten as

$$\vec{x}_t \cdot \vec{\nu} = -\Delta_s \varkappa, \quad \varkappa\vec{\nu} = \Delta_s \vec{x}. \tag{1.11}$$

We remark that a surface that encloses a region in $\mathbb{R}^d$ and evolves according to (1.2) conserves volume. Choosing $\vec{\nu}$ from now on to be the outward unit normal to the region and taking $\mathrm{Vol}(\Gamma(t))$ as the total enclosed volume, the above statement follows from

$$\frac{\mathrm{d}}{\mathrm{d}t}[\mathrm{Vol}(\Gamma(t))] = \int_\Gamma \mathcal{V}\,\mathrm{d}s = -\int_\Gamma \Delta_s \varkappa\,\mathrm{d}s = 0,$$

where the last identity follows from the Gauss theorem on manifolds. Furthermore the total surface area, $|\Gamma(t)|$, decreases in time as can be seen from

$$\frac{\mathrm{d}}{\mathrm{d}t}|\Gamma(t)| = -\int_\Gamma \varkappa\mathcal{V}\,\mathrm{d}s = \int_\Gamma \varkappa(\Delta_s\varkappa)\mathrm{d}s = -\int_\Gamma (\nabla_s\varkappa)^2\,\mathrm{d}s \leqslant 0,$$

where $\nabla_s f = \nabla f - (\vec{\nu}\cdot\nabla f)\vec{\nu}$ is the tangential gradient on Γ; see e.g. [10, p. 150]. For an overview on existing approaches to approximate geometric evolution equations, including parametric, level-set and phase-field methods, we refer also to this recent review article. We remark that for the evolution of surfaces the question, whether the continuous case arises as the limit of its discrete approximations, is not well developed. However, for the time-independent case, certain results exist, see e.g. [31,18] and the references therein.

This paper is organised as follows. In Section 2, we will consider a fully discrete finite element approximation of a variational formulation of (1.11), as well as (1.7), (1.8) and (1.10), where throughout we will restrict our attention to the evolution of closed hypersurfaces in $\mathbb{R}^d$ with $d = 3$. In addition, we demonstrate the well posedness of these approximations and derive stability bounds. In Section 4, we consider the corresponding semidiscrete finite element approximations and prove that here the induced tangential motion gives rise to "conformal polyhedral surfaces". This result can be seen as a generalization of the equidistribution property established for the planar case ($d = 2$) in [7,5]. Finally, in Section 5 we present a large number of numerical computations and compare our results, where possible, with those from other parametric algorithms in the literature.

2. Finite element approximation

We introduce the following finite element approximation, based on the seminal paper by [12]. Let $0 = t_0 < t_1 < \cdots < t_{M-1} < t_M = T$ be a partitioning of $[0, T]$ into possibly variable time steps $\tau_m := t_{m+1} - t_m$, $m = 0 \to M-1$. We set $\tau := \max_{m=0\to M-1}\tau_m$. Let Γ^m be a *polyhedral surface*, i.e. a union of non-degenerate triangles with no hanging vertices (see [10, p. 164]), approximating the closed surface $\Gamma(t_m)$, $m = 0 \to M$. Following [12], we now parameterize the new closed surface Γ^{m+1} over Γ^m. Hence, given $\vec{X}^m$, a parameterization of Γ^m, we introduce the following finite element spaces. Let $\Gamma^m = \bigcup_{j=1}^J \overline{\sigma_j^m}$, where $\{\sigma_j^m\}_{j=1}^J$ is a family of mutually disjoint open triangles with vertices $\{\vec{q}_k^m\}_{k=1}^K$ and set $h := \max_{j=1\to J}\mathrm{diam}(\sigma_j^m)$. Then for $m = 0 \to M-1$, let

$$\underline{V}(\Gamma^m) := \{\vec{\chi} \in C(\Gamma^m, \mathbb{R}^3) : \vec{\chi}|_{\sigma_j^m} \text{ is linear } \forall j = 1 \to J\} := [W(\Gamma^m)]^3 \subset H^1(\Gamma^m, \mathbb{R}^3), \tag{2.1}$$

where $W(\Gamma^m) \subset H^1(\Gamma^m, \mathbb{R})$ is the space of scalar continuous piecewise linear functions on Γ^m, with $\{\phi_k^m\}_{k=1}^K$ denoting the standard basis of $W(\Gamma^m)$.

For scalar and vector functions $u, v \in L^2(\Gamma^m, \mathbb{R}^{(3)})$ we introduce the L^2 inner product $\langle\cdot,\cdot\rangle_m$ over the current polyhedral surface Γ^m, which is described by the vector function $\vec{X}^m$, as follows

$$\langle u, v\rangle_m := \int_{\Gamma^m} u \cdot v\,\mathrm{d}s.$$

Here and throughout this paper, $\cdot^{(*)}$ denotes an expression with or without the superscript $*$, and similarly for subscripts. We note that for $m \geqslant 1$, $\vec{X}^m \in \underline{V}(\Gamma^{m-1})$ and for $m \geqslant 0$ we will denote also the identity function, id, on Γ^m as $\vec{X}^m$. This slight abuse of notation will be used throughout the paper.

If u, v are piecewise continuous, with possible jumps across the edges of $\{\sigma_j^m\}_{j=1}^J$, we introduce the mass lumped inner product $\langle\cdot,\cdot\rangle_m^h$ as

$$\langle u, v\rangle_m^h := \frac{1}{3}\sum_{j=1}^{J} |\sigma_j^m| \sum_{k=0}^{2} (u\cdot v)((\vec{q}_{j_k}^m)^-), \tag{2.2}$$

where $\{\vec{q}_{j_k}^m\}_{k=0}^2$ are the vertices of σ_j^m, i.e. $\overline{\sigma_j^m} = \Delta\{\vec{q}_{j_k}^m\}_{k=0}^2$, and where we define $u((\vec{q}_{j_k}^m)^-) := \lim_{\sigma_j^m \ni \vec{p} \to \vec{q}_{j_k}^m} u(\vec{p})$. Here $|\sigma_j^m| = \frac{1}{2}|(\vec{q}_{j_1}^m - \vec{q}_{j_0}^m) \times (\vec{q}_{j_2}^m - \vec{q}_{j_0}^m)|$ is the measure of σ_j^m. In addition, we introduce the outward unit normal $\vec{\nu}^m$ to Γ^m; that is,

$$\vec{\nu}_j^m := \vec{\nu}^m|_{\sigma_j^m} := \frac{(\vec{q}_{j_1}^m - \vec{q}_{j_0}^m) \times (\vec{q}_{j_2}^m - \vec{q}_{j_0}^m)}{|(\vec{q}_{j_1}^m - \vec{q}_{j_0}^m) \times (\vec{q}_{j_2}^m - \vec{q}_{j_0}^m)|}, \tag{2.3}$$

where we have assumed that the vertices $\{\vec{q}_{j_k}^m\}_{k=0}^2$ are ordered anti-clockwise on the outer surface of σ_j^m. Finally, we set $|\cdot|_{m,h}^2 := \langle\cdot,\cdot\rangle_m^{(h)}$.

We propose the following approximation to (1.7): Given Γ^0 and the identity function $\vec{X}^0 \in \underline{V}(\Gamma^0)$ on Γ^0, then for $m = 0 \to M-1$ find $\{\vec{X}^{m+1}, \kappa^{m+1}\} \in \underline{V}(\Gamma^m) \times W(\Gamma^m)$ such that

$$\left\langle \frac{\vec{X}^{m+1} - \vec{X}^m}{\tau_m}, \chi\vec{\nu}^m \right\rangle_m^h - \langle f(\kappa^{m+1}), \chi\rangle_m^h = 0 \quad \forall \chi \in W(\Gamma^m), \tag{2.4a}$$

$$\langle \kappa^{m+1}\vec{\nu}^m, \vec{\eta}\rangle_m^h + \langle \nabla_s \vec{X}^{m+1}, \nabla_s \vec{\eta}\rangle_m = 0 \quad \forall \vec{\eta} \in \underline{V}(\Gamma^m), \tag{2.4b}$$

where, as noted above, the inner products $\langle\cdot,\cdot\rangle_m^{(h)}$ as well as ∇_s depend on m.

In order to approximate (1.8), we adapt (2.4a) to

$$\left\langle \frac{\vec{X}^{m+1} - \vec{X}^m}{\tau_m}, \chi\vec{\nu}^m \right\rangle_m^h - \langle f(\kappa^{m+1}), \chi\rangle_m^h = -\frac{\langle f(\kappa^m), 1\rangle_m^h}{\langle 1, 1\rangle_m} \langle 1, \chi\rangle_m \quad \forall \chi \in W(\Gamma^m), \tag{2.5}$$

with a suitable choice for $\kappa^0 \in W(\Gamma^0)$, see Section 5. Note that here and throughout, as no confusion can arise, we denote by κ^m the function $z \in W(\Gamma^m)$, defined by $z(\vec{q}_k^m) = \kappa^m(\vec{q}_k^{m-1})$, $k = 1 \to K$, where $\kappa^m \in W(\Gamma^{m-1})$ is given.

Moreover, we propose the following approximation to (1.11): Given Γ^0 and the identity function $\vec{X}^0 \in \underline{V}(\Gamma^0)$ on Γ^0, then for $m = 0 \to M-1$ find $\{\vec{X}^{m+1}, \kappa^{m+1}\} \in \underline{V}(\Gamma^m) \times W(\Gamma^m)$ such that

$$\left\langle \frac{\vec{X}^{m+1} - \vec{X}^m}{\tau_m}, \chi\vec{\nu}^m \right\rangle_m^h - \langle \nabla_s \kappa^{m+1}, \nabla_s \chi\rangle_m = 0 \quad \forall \chi \in W(\Gamma^m), \tag{2.6a}$$

$$\langle \kappa^{m+1}\vec{\nu}^m, \vec{\eta}\rangle_m^h + \langle \nabla_s \vec{X}^{m+1}, \nabla_s \vec{\eta}\rangle_m = 0 \quad \forall \vec{\eta} \in \underline{V}(\Gamma^m). \tag{2.6b}$$

Before we can proceed to prove existence and uniqueness to these approximations, we have to make the following very mild assumption on the triangulations at each time level.

($\mathcal{A}$) We assume for $m = 0 \to M$ that $|\sigma_j^m| > 0$ for all $j = 1 \to J$. For $k = 1 \to K$, let $\mathcal{T}_k^m := \{\sigma_j^m : \vec{q}_k^m \in \overline{\sigma_j^m}\}$ and set

$$\Lambda_k^m := \cup_{\sigma_j^m \in \mathcal{T}_k^m} \overline{\sigma_j^m} \quad \text{and} \quad \vec{\omega}_k^m := \frac{1}{|\Lambda_k^m|} \sum_{\sigma_j^m \in \mathcal{T}_k^m} |\sigma_j^m| \vec{\nu}_j^m. \tag{2.7}$$

Then we further assume that $\dim \operatorname{span}\{\vec{\omega}_k^m\}_{k=1}^K = d = 3$, $m = 0 \to M-1$.

Remark 2.1. We note that one can interpret $\vec{\omega}_k^m$ as a weighted normal defined at the node $\vec{X}^m(\vec{q}_k^m) = \vec{q}_k^m$ of the surface Γ^m, where in general $|\vec{\omega}_k^m| < 1$. In addition, we note that ($\mathcal{A}$) is only violated in very rare occasions. For example, it always holds for surfaces without self intersections.

Theorem 2.1. *Let the assumption* $(\mathcal{A})$ *hold. Then there exists a unique solution* $\{\vec{X}^{m+1}, \kappa^{m+1}\} \in \underline{V}(\Gamma^m) \times W(\Gamma^m)$ *to the system (2.6a), (2.6b); and to (2.4a), (2.4b) on assuming that* $f : (a,b) \to \mathbb{R}$ *with* $-\infty \leqslant a < 0 < b \leqslant \infty$ *is strictly increasing, continuous and such that* $f((a,b)) = \mathbb{R}$.

Proof. We first discuss (2.6a) and (2.6b), which requires a linear system to be solved at each time level. Hence existence follows from uniqueness. To investigate the latter, we consider the system: Find $\{\vec{X}, \kappa\} \in \underline{V}(\Gamma^m) \times W(\Gamma^m)$ such that

$$\langle \vec{X}, \chi \vec{\nu}^m \rangle_m^h - \tau_m \langle \nabla_s \kappa, \nabla_s \chi \rangle_m = 0 \quad \forall \chi \in W(\Gamma^m), \tag{2.8a}$$

$$\langle \kappa \vec{\nu}^m, \vec{\eta} \rangle_m^h + \langle \nabla_s \vec{X}, \nabla_s \vec{\eta} \rangle_m = 0 \quad \forall \vec{\eta} \in \underline{V}(\Gamma^m). \tag{2.8b}$$

Choosing $\chi \equiv \kappa \in W(\Gamma^m)$ in (2.8a) and $\vec{\eta} \equiv \vec{X} \in \underline{V}(\Gamma^m)$ in (2.8b) yields that

$$|\nabla_s \vec{X}|_m^2 + \tau_m |\nabla_s \kappa|_m^2 = 0. \tag{2.9}$$

It follows from (2.9) that $\kappa \equiv \kappa^c \in \mathbb{R}$ and $\vec{X} \equiv \vec{X}^c \in \mathbb{R}^3$; and hence that

$$\langle \vec{X}^c, \chi \vec{\nu}^m \rangle_m^h = 0 \quad \forall \chi \in W(\Gamma^m), \qquad \kappa^c \langle \vec{\nu}^m, \vec{\eta} \rangle_m^h = 0 \quad \forall \vec{\eta} \in \underline{V}(\Gamma^m). \tag{2.10}$$

Choosing $\vec{\eta} \equiv \vec{z} \phi_k^m \in \underline{V}(\Gamma^m)$ in (2.10), and noting (2.2) and (2.7), yields, on assuming $\kappa^c \neq 0$, that for $k = 1 \to K$

$$\vec{\omega}_k^m \cdot \vec{z} = 0 \quad \forall \vec{z} \in \mathbb{R}^3 \quad \Longleftrightarrow \quad \vec{\omega}_k^m = \vec{0}. \tag{2.11}$$

However, this contradicts assumption $(\mathcal{A})$ and hence $\kappa^c = 0$. Similarly, choosing $\chi \equiv \phi_k^m$ in (2.10) yields that $\vec{X}^c \cdot \vec{\omega}_k^m = 0$ for $k = 1 \to K$. It follows from assumption $(\mathcal{A})$ that $\vec{X}^c \equiv \vec{0}$. Hence we have shown that there exists a unique solution $\{\vec{X}^{m+1}, \kappa^{m+1}\} \in \underline{V}(\Gamma^m) \times W(\Gamma^m)$ to (2.6a), (2.6b).

For a general function $f : (a,b) \to \mathbb{R}$ fulfilling the assumptions of the theorem, we can rewrite (2.4a) and (2.4b), on noting (2.2) and (2.7), as: Find $\vec{X}^{m+1} \in \underline{V}(\Gamma^m)$ such that

$$\langle \nabla_s \vec{X}^{m+1}, \nabla_s \vec{\eta} \rangle_m + \left\langle f^{-1}\left(\frac{\vec{X}^{m+1} - \vec{X}^m}{\tau_m} \cdot \vec{\omega}^m \right), \vec{\eta} \cdot \vec{\omega}^m \right\rangle_m^h = 0 \quad \forall \vec{\eta} \in \underline{V}(\Gamma^m), \tag{2.12}$$

where $\vec{\omega}^m := \sum_{k=1}^K \vec{\omega}_k^m \phi_k^m$. Then $\kappa^{m+1} \in W(\Gamma^m)$ is uniquely determined from

$$\kappa^{m+1}(\vec{q}_k^m) = f^{-1}\left(\frac{\vec{X}^{m+1}(\vec{q}_k^m) - \vec{X}^m(\vec{q}_k^m)}{\tau_m} \cdot \vec{\omega}_k^m \right) \qquad k = 1 \to K. \tag{2.13}$$

It follows that (2.12) is the Euler–Lagrange variation of the strictly convex minimization problem:

$$\min_{\vec{\eta} \in \underline{V}(\Gamma^m)} \left[\frac{1}{2} |\nabla_s \vec{\eta}|_m^2 + \tau_m \left\langle \Phi\left(\frac{\vec{\eta} - \vec{X}^m}{\tau_m} \cdot \vec{\omega}^m \right), 1 \right\rangle_m^h \right], \tag{2.14}$$

where Φ is an anti-derivative of f^{-1}. We note that $\Phi : \mathbb{R} \to \mathbb{R}$ is strictly convex with $\Phi'(f(0)) = f^{-1}(f(0)) = 0$ and hence we obtain that Φ is bounded from below and is coercive. Therefore there exists a unique solution $\vec{X}^{m+1} \in \underline{V}(\Gamma^m)$ to (2.12), and hence a unique solution $\{\vec{X}^{m+1}, \kappa^{m+1}\} \in \underline{V}(\Gamma^m) \times W(\Gamma^m)$ to (2.4a) and (2.4b). □

The above proof immediately applies to the case when (2.4a) is replaced by (2.5). We remark also that we still obtain uniqueness for strictly increasing continuous functions $f : (a,b) \to \mathbb{R}$ with $-\infty \leqslant a < b \leqslant \infty$. This follows, since Φ defined as above is still strictly convex. Existence cannot be established as easily as above, because Φ is not coercive any longer. This discussion is relevant, e.g. for $f(r) = -r^{-1}$ with $r \in (-\infty, 0)$, which is the case of the inverse mean curvature flow if $\varkappa(\cdot, 0) < 0$. In this case we obtain that $\Phi : (0, \infty) \to \mathbb{R}$ is defined as $\Phi(r) = -\ln r$.

In order to establish that our schemes are unconditionally stable, we introduce the following lemma.

Lemma 2.1. *Let $\Upsilon = \bigcup_{j=1}^{J} \overline{\sigma}_j$ be a polyhedral surface. Then we have for all j that*

$$\frac{1}{2}\int_{\sigma_j} |\nabla_s \vec{\mathrm{id}}|^2 \mathrm{d}s = |\sigma_j| \quad \text{and} \quad \frac{1}{2}\int_{\sigma_j} |\nabla_s \vec{Y}|^2 \mathrm{d}s \geqslant |\vec{Y}(\sigma_j)| \quad \forall \vec{Y} \in \underline{V}(\Upsilon). \tag{2.15}$$

Proof. It holds that

$$|\vec{Y}(\sigma_j)| = \int_{\sigma_j} \left| \frac{\partial \vec{Y}}{\partial \vec{\rho}_1} \times \frac{\partial \vec{Y}}{\partial \vec{\rho}_2} \right| \mathrm{d}s, \tag{2.16}$$

where $\{\vec{\rho}_1, \vec{\rho}_2\}$ is an orthonormal basis for the plane containing σ_j. Hence we have that

$$\nabla_s \vec{Y} = \sum_{i=1}^{2} \frac{\partial \vec{Y}}{\partial \vec{\rho}_i} \otimes \vec{\rho}_i \quad \text{and} \quad |\nabla_s \vec{Y}|^2 = \sum_{i=1}^{2} \left| \frac{\partial \vec{Y}}{\partial \vec{\rho}_i} \right|^2 \quad \text{on } \sigma_j. \tag{2.17}$$

Next we note that

$$|\vec{a} \times \vec{b}| \leqslant |\vec{a}||\vec{b}| \leqslant \frac{1}{2}(|\vec{a}|^2 + |\vec{b}|^2) \quad \forall \vec{a}, \vec{b} \in \mathbb{R}^3, \tag{2.18}$$

with equality if and only if $\vec{a} \cdot \vec{b} = 0$ and $|\vec{a}| = |\vec{b}|$. The desired results (2.15) then follow immediately on combining (2.16), (2.17) and (2.18); and noting that if $\vec{Y}$ is the identity function on σ_j, then $\frac{\partial \vec{Y}}{\partial \vec{\rho}_i}|_{\sigma_j} = \vec{\rho}_i$. □

Theorem 2.2. *Let the assumptions ($\mathcal{A}$) hold, and $\{\vec{X}^m, \kappa^m\}_{m=1}^{M}$ be the unique solution to (2.6a) and (2.6b). Then for $k = 1 \to M$ we have that*

$$|\Gamma^k| + \sum_{m=0}^{k-1} \left(\tau_m |\nabla_s \kappa^{m+1}|_m^2 + \frac{1}{2} |\nabla_s (\vec{X}^{m+1} - \vec{X}^m)|_m^2 \right) \leqslant |\Gamma^0|. \tag{2.19}$$

Proof. Choosing $\chi \equiv \kappa^{m+1} \in W(\Gamma^m)$ in (2.6a) and $\vec{\eta} \equiv \frac{\vec{X}^{m+1} - \vec{X}^m}{\tau_m} \in \underline{V}(\Gamma^m)$ in (2.6b) yields that

$$\langle \nabla_s \vec{X}^{m+1}, \nabla_s (\vec{X}^{m+1} - \vec{X}^m) \rangle_m + \tau_m |\nabla_s \kappa^{m+1}|_m^2 = 0. \tag{2.20}$$

On noting (2.15), and as $\vec{X}^m \equiv \vec{\mathrm{id}}$ on Γ^m, we have that

$$\begin{aligned} \langle \nabla_s \vec{X}^{m+1}, \nabla_s (\vec{X}^{m+1} - \vec{X}^m) \rangle_m &= \frac{1}{2} \left[|\nabla_s \vec{X}^{m+1}|_m^2 - |\nabla_s \vec{X}^m|_m^2 + |\nabla_s (\vec{X}^{m+1} - \vec{X}^m)|_m^2 \right] \\ &\geqslant |\Gamma^{m+1}| - |\Gamma^m| + \frac{1}{2} |\nabla_s (\vec{X}^{m+1} - \vec{X}^m)|_m^2. \end{aligned} \tag{2.21}$$

Combining (2.20) and (2.21) yields that

$$|\Gamma^{m+1}| - |\Gamma^m| + \tau_m |\nabla_s \kappa^{m+1}|_m^2 + \frac{1}{2} |\nabla_s (\vec{X}^{m+1} - \vec{X}^m)|_m^2 \leqslant 0. \tag{2.22}$$

Summing (2.22) for $m = 0 \to k-1$ yields the desired result. □

A different proof of the above stability result can be given based on [3, Lemma 1], see e.g. [4, Theorem 2.1].

In addition, stability results for (2.4a) and (2.4b) and the variants involving (2.5) can be established in certain cases. For example, the term $|\nabla_s \kappa^{m+1}|_m^2$ in (2.19) is replaced by $\langle f(\kappa^{m+1}), \kappa^{m+1} \rangle_m^h$, which once again is non-negative if f is monotonically increasing with $f(0) = 0$. Of course, it may be computationally more convenient to consider a linearized version of (2.4a). For example, for (1.5) with $\beta \geqslant 1$ one could replace (2.4a) by

$$\left\langle \frac{\vec{X}^{m+1} - \vec{X}^m}{\tau_m}, \chi \vec{\nu}^m \right\rangle_m^h - \left\langle \frac{f(\kappa^m)}{\kappa^m} \kappa^{m+1}, \chi \right\rangle_m^h = 0 \quad \forall \chi \in W(\Gamma^m). \tag{2.23}$$

Once again, it is then straightforward to prove existence and uniqueness, and derive a stability result for this scheme.

Remark 2.2. In Section 5, we will report on computations for our approximations to (1.3) and (1.2), i.e. (2.4a), (2.4b) and (2.6a), (2.6b), and compare our results with two other schemes in the literature. The first scheme approximates mean curvature flow, (1.3). It was introduced in [12] and can be formulated as: Find $\vec{X}^{m+1} \in \underline{V}(\Gamma^m)$ such that

$$\left\langle \frac{\vec{X}^{m+1}-\vec{X}^m}{\tau_m}, \vec{\eta} \right\rangle_m^h + \langle \nabla_s \vec{X}^{m+1}, \nabla_s \vec{\eta} \rangle_m = 0 \quad \forall \vec{\eta} \in \underline{V}(\Gamma^m). \tag{2.24}$$

The system (2.24) is a discretization of the variational formulation of

$$\vec{x}_t = \vec{\varkappa}, \qquad \vec{\varkappa} := \varkappa \vec{\nu} = \Delta_s \vec{x},$$

as opposed to (1.7) with $f(r) := r$. From (2.12), we see that our scheme (2.4a) and (2.4b) with $f(r) := r$ can be rewritten as: Find $\vec{X}^{m+1} \in \underline{V}(\Gamma^m)$ such that

$$\left\langle \frac{\vec{X}^{m+1}-\vec{X}^m}{\tau_m} \cdot \vec{\omega}^m, \vec{\eta} \cdot \vec{\omega}^m \right\rangle_m^h + \langle \nabla_s \vec{X}^{m+1}, \nabla_s \vec{\eta} \rangle_m = 0 \quad \forall \vec{\eta} \in \underline{V}(\Gamma^m), \tag{2.25}$$

which clearly highlights the key difference between the two schemes. The second scheme approximates surface diffusion, (1.2). It is from [4] and can be stated as: Let $\vec{X}^{m+1} := \vec{X}^m + \tau_m \vec{V}^{m+1}$, where $\vec{V}^{m+1} \in \underline{V}(\Gamma^m)$ is part of the solution of: Find $\{\vec{V}^{m+1}, \kappa^{m+1}, \vec{\kappa}^{m+1}, V^{m+1}\} \in \underline{V}(\Gamma^m) \times W(\Gamma^m) \times \underline{V}(\Gamma^m) \times W(\Gamma^m)$ such that

$$\langle \vec{\kappa}^{m+1}, \vec{\eta} \rangle_m + \tau_m \langle \nabla_s \vec{V}^{m+1}, \nabla_s \vec{\eta} \rangle_m = -\langle \nabla_s \vec{X}^m, \nabla_s \vec{\eta} \rangle_m \quad \forall \vec{\eta} \in \underline{V}(\Gamma^m), \tag{2.26a}$$

$$\langle \kappa^{m+1}, \chi \rangle_m - \langle \vec{\kappa}^{m+1}, \chi \vec{\nu}^m \rangle_m = 0 \quad \forall \chi \in W(\Gamma^m), \tag{2.26b}$$

$$\langle V^{m+1}, \chi \rangle_m - \langle \nabla_s \kappa^{m+1}, \nabla_s \chi \rangle_m = 0 \quad \forall \chi \in W(\Gamma^m), \tag{2.26c}$$

$$\langle \vec{V}^{m+1}, \vec{\eta} \rangle_m - \langle V^{m+1} \vec{\nu}^m, \vec{\eta} \rangle_m = 0 \quad \forall \vec{\eta} \in \underline{V}(\Gamma^m). \tag{2.26d}$$

The system (2.26a)–(2.26d) is a discretization of the variational formulation of

$$\vec{\varkappa} = \Delta_s \vec{x}, \quad \varkappa = \vec{\varkappa} \cdot \vec{\nu}, \quad v = -\Delta_s \varkappa, \quad \vec{x}_t = \vec{v} = v\vec{\nu}$$

as opposed to (1.11). We note that both schemes (2.24) and (2.26a)–(2.26d) only change the approximation of $\vec{x}$ in the normal direction, whereas the schemes proposed in this paper also induce tangential changes. This is a crucial difference.

Finally, we consider the intermediate motion (1.10), to which we introduce the following approximation. Given Γ^0 and the identity function $\vec{X}^0 \in \underline{V}(\Gamma^0)$ on Γ^0, then for $m = 0 \to M-1$ find $\{\vec{X}^{m+1}, Y^{m+1}, \kappa^{m+1}\} \in \underline{V}(\Gamma^m) \times [W(\Gamma^m)]^2$ such that

$$\left\langle \frac{\vec{X}^{m+1}-\vec{X}^m}{\tau_m}, \chi \vec{\nu}^m \right\rangle_m^h - \langle \nabla_s Y^{m+1}, \nabla_s \chi \rangle_m = 0 \quad \forall \chi \in W(\Gamma^m), \tag{2.27a}$$

$$\frac{1}{\xi} \langle \nabla_s Y^{m+1}, \nabla_s \chi \rangle_m + \frac{1}{\alpha} \langle Y^{m+1}, \chi \rangle_m^h - \langle \kappa^{m+1}, \chi \rangle_m^h = 0 \quad \forall \chi \in W(\Gamma^m), \tag{2.27b}$$

$$\langle \kappa^{m+1} \vec{\nu}^m, \vec{\eta} \rangle_m^h + \langle \nabla_s \vec{X}^{m+1}, \nabla_s \vec{\eta} \rangle_m = 0 \quad \forall \vec{\eta} \in \underline{V}(\Gamma^m). \tag{2.27c}$$

Theorem 2.3. *Let the assumption* $(\mathcal{A})$ *hold. Then there exists a unique solution* $\{\vec{X}^{m+1}, Y^{m+1}, \kappa^{m+1}\} \in \underline{V}(\Gamma^m) \times [W(\Gamma^m)]^2$ *to the system* (2.27a)–(2.27c). *Moreover, we have for* $k = 1 \to M$ *that*

$$|\Gamma^k| + \frac{1}{\alpha} \sum_{m=0}^{k-1} \tau_m |\nabla_s Y^{m+1}|_m^2 + \xi \sum_{m=0}^{k-1} \tau_m |\kappa^{m+1} - \frac{1}{\alpha} Y^{m+1}|_{m,h}^2 \leqslant |\Gamma^0|. \tag{2.28}$$

Proof. The uniqueness proof is a straightforward adaption of the proof to Theorem 2.1. As (2.27a)–(2.27c) is linear, existence follows from uniqueness, and the latter is easily established for the relevant equations

$$\langle\vec{X},\chi\vec{\nu}^m\rangle^h_m-\tau_m\langle\nabla_s Y,\nabla_s\chi\rangle_m=0\quad\forall\chi\in W(\Gamma^m),$$
$$\frac{1}{\xi}\langle\nabla_s Y,\nabla_s\chi\rangle_m+\frac{1}{\alpha}\langle Y,\chi\rangle^h_m-\langle\kappa,\chi\rangle^h_m=0\quad\forall\chi\in W(\Gamma^m),$$
$$\langle\kappa\vec{\nu}^m,\vec{\eta}\rangle^h_m+\langle\nabla_s\vec{X},\nabla_s\vec{\eta}\rangle_m=0\quad\forall\vec{\eta}\in\underline{V}(\Gamma^m);$$

on choosing $\chi=\frac{\alpha}{\xi}\kappa$, $\chi=\tau_m(\alpha\kappa-Y)$ and $\vec{\eta}=\frac{\alpha}{\xi}\vec{X}$, respectively. Combining yields that

$$\frac{\alpha}{\xi}|\nabla_s\vec{X}|^2_m+\frac{\tau_m}{\xi}|\nabla_s Y|^2_m+\frac{\tau_m}{\alpha}|\alpha\kappa-Y|^2_{m,h}=0. \tag{2.29}$$

It follows from (2.29) that $\vec{X}=\vec{X}^c\in\mathbb{R}^3$, $Y=Y^c\in\mathbb{R}$ and $\kappa=\frac{Y^c}{\alpha}\in\mathbb{R}$, and hence, similarly to (2.10) on recalling assumption $(\mathcal{A})$ that $\vec{X}^c=\vec{0}$ and $Y^c=0$. Hence we have existence of a unique solution $\{\vec{X}^{m+1},Y^{m+1},\kappa^{m+1}\}\in\underline{V}(\Gamma^m)\times[W(\Gamma^m)]^2$ to the system (2.27a)–(2.27c). Finally, choosing $\chi=\frac{\alpha}{\xi}\kappa^{m+1}$, $\chi=\tau_m(\alpha\kappa^{m+1}-Y^{m+1})$ and $\vec{\eta}=\frac{\alpha}{\xi}(\vec{X}^{m+1}-\vec{X}^m)$ in (2.27a)–(2.27c) gives, similarly to (2.29), that

$$\langle\nabla_s\vec{X}^{m+1},\nabla_s(\vec{X}^{m+1}-\vec{X}^m)\rangle_m+\frac{\tau_m}{\alpha}|\nabla_s Y^{m+1}|^2_m+\xi\tau_m|\kappa^{m+1}-\frac{1}{\alpha}Y^{m+1}|^2_{m,h}=0. \tag{2.30}$$

Combining (3.10) and (2.21) yields (2.28). □

3. Solution of the algebraic equations

In order to solve the (nonlinear) algebraic systems arising from (2.4a) and (2.4b), its generalisations, (2.6a), (2.6b) and (2.27a)–(2.27c), we apply a Schur complement approach. For ease of exposition, we describe it first for (2.4a) and (2.4b) when $f(r):=r$. Here and throughout, for a given $n\in\mathbb{N}$, let $\vec{Id}_n\in(\mathbb{R}^{3\times3})^{n\times n}$ be the identity matrix, and similarly for $Id_n\in\mathbb{R}^{n\times n}$. We introduce also the matrices $\vec{N}_m\in(\mathbb{R}^3)^{K\times K}$, $M_m,A_m\in\mathbb{R}^{K\times K}$ and $\vec{A}_m\in(\mathbb{R}^{3\times3})^{K\times K}$ with entries

$$[M_m]_{kl}:=\langle\phi^m_k,\phi^m_l\rangle^h_m,\quad[\vec{N}_m]_{kl}:=\int_{\Gamma^m}\pi^h[\phi^m_k\phi^m_l]\vec{\nu}^m\,\mathrm{d}s,\quad[A_m]_{kl}:=\langle\nabla_s\phi^m_k,\nabla_s\phi^m_l\rangle_m \tag{3.1}$$

and $[\vec{A}_m]_{kl}:=[A_m]_{kl}\vec{Id}_1$, where $\pi^h:C(\Gamma^m,\mathbb{R})\to W(\Gamma^m)$ is the standard interpolation operator at the nodes $\{\vec{q}^m_k\}_{k=1}^K$. We can then formulate (2.4a) and (2.4b) with $f(r):=r$ as: Find $\{\delta\vec{X}^{m+1},\kappa^{m+1}\}\in(\mathbb{R}^3)^K\times\mathbb{R}^K$ such that

$$\begin{pmatrix}\tau_m M_m & -\vec{N}^T_m\\ \vec{N}_m & \vec{A}_m\end{pmatrix}\begin{pmatrix}\kappa^{m+1}\\ \delta\vec{X}^{m+1}\end{pmatrix}=\begin{pmatrix}0\\ -\vec{A}_m\vec{X}^m\end{pmatrix}, \tag{3.2}$$

where, with the obvious abuse of notation, $\delta\vec{X}^{m+1}=(\delta\vec{X}^{m+1}_1,\dots,\delta\vec{X}^{m+1}_K)^T$ and $\kappa^{m+1}=(\kappa^{m+1}_1,\dots,\kappa^{m+1}_K)^T$ are the vectors of coefficients with respect to the standard basis for $\vec{X}^{m+1}-\vec{X}^m$ and κ^{m+1}, respectively. We can transform (3.2) to

$$\kappa^{m+1}=\frac{1}{\tau_m}M^{-1}_m\vec{N}^T_m\delta\vec{X}^{m+1}, \tag{3.3a}$$
$$\left(\vec{A}_m+\frac{1}{\tau_m}\vec{N}_m M^{-1}_m\vec{N}^T_m\right)\delta\vec{X}^{m+1}=-\vec{A}_m\vec{X}^m. \tag{3.3b}$$

As (3.3b) is clearly symmetric and positive definite under our assumption $(\mathcal{A})$, there exists a unique solution to (3.3b). Moreover, the solution to (3.3a) and (3.3b) uniquely solves (2.4a) and (2.4b) with $f(r):=r$.

We note that for the approximation (2.4a) and (2.4b) with nonlinear f, the linear Schur system (3.3a) and (3.3b) has to be replaced by the corresponding nonlinear system:

$$\kappa^{m+1}=f^{-1}\left[\frac{1}{\tau_m}M^{-1}_m\vec{N}^T_m\delta\vec{X}^{m+1}\right], \tag{3.4a}$$
$$\vec{A}_m\delta\vec{X}^{m+1}+\vec{N}_m f^{-1}\left[\frac{1}{\tau_m}M^{-1}_m\vec{N}^T_m\delta\vec{X}^{m+1}\right]=-\vec{A}_m\vec{X}^m, \tag{3.4b}$$

where $f^{-1}(z) \in \mathbb{R}^K$ is defined by $[f^{-1}(z)]_i := f^{-1}(z_i)$, $i = 1 \to K$, for any $z \in \mathbb{R}^K$. In addition, the scheme (2.5) and (2.4b) can be solved by

$$\kappa^{m+1} = f^{-1}\left[\frac{1}{\tau_m} M_m^{-1} \vec{N}_m^T \delta\vec{X}^{m+1} + \lambda_m 1\right],$$

$$\vec{A}_m \delta\vec{X}^{m+1} + \vec{N}_m f^{-1}\left[\frac{1}{\tau_m} M_m^{-1} \vec{N}_m^T \delta\vec{X}^{m+1} + \lambda_m 1\right] = -\vec{A}_m \vec{X}^m,$$

where $\lambda_m := \frac{\langle f(\kappa^m), 1\rangle_m^h}{\langle 1, 1\rangle_m} \in \mathbb{R}$ and $1 := (1, \ldots, 1)^T \in \mathbb{R}^K$.

Similarly, (2.6a) and (2.6b) can be reformulated as: Find $\{\delta\vec{X}^{m+1}, \kappa^{m+1}\} \in (\mathbb{R}^3)^K \times \mathbb{R}^K$, such that

$$\begin{pmatrix} \tau_m A_m & -\vec{N}_m^T \\ \vec{N}_m & \vec{A}_m \end{pmatrix} \begin{pmatrix} \kappa^{m+1} \\ \delta\vec{X}^{m+1} \end{pmatrix} = \begin{pmatrix} 0 \\ -\vec{A}_m \vec{X}^m \end{pmatrix}. \tag{3.5}$$

Introducing the inverse S_m of A_m restricted on the set $(\ker A_m)^\perp \equiv (\mathrm{span}\{1\})^\perp$ and noting that the first equation in (3.5) implies $1^T \vec{N}_m^T \delta\vec{X}^{m+1} = 0$, one can transform (3.5) to

$$\kappa^{m+1} = \frac{1}{\tau_m} S_m \vec{N}_m^T \delta\vec{X}^{m+1} + \mu 1, \tag{3.6a}$$

$$\left(\vec{A}_m + \frac{1}{\tau_m} \vec{N}_m S_m \vec{N}_m^T\right) \delta\vec{X}^{m+1} = -\vec{A}_m \vec{X}^m - \mu \vec{N}_m 1, \quad (\delta\vec{X}^{m+1})^T \vec{N}_m 1 = 0, \tag{3.6b}$$

where $\mu = \frac{1^T \kappa^{m+1}}{1^T 1} \in \mathbb{R}$ is unknown. We introduce also the orthogonal projection $\vec{\Pi}_m$ onto $\mathcal{R}_m^\perp := \{\vec{X} \in (\mathbb{R}^3)^K : \vec{X}^T \vec{N}_m 1 = 0\}$ by $\vec{\Pi}_m := \vec{Id}_K - \frac{\vec{w}\vec{w}^T}{\vec{w}^T \vec{w}}$, where $\vec{w} := \vec{N}_m 1$. Then (3.6b), on noting that $\vec{\Pi}_m \delta\vec{X}^{m+1} = \delta\vec{X}^{m+1}$, is replaced by

$$\vec{\Pi}_m \left(\vec{A}_m + \frac{1}{\tau_m} \vec{N}_m S_m \vec{N}_m^T\right) \vec{\Pi}_m \delta\vec{X}^{m+1} = -\vec{\Pi}_m \vec{A}_m \vec{X}^m. \tag{3.7}$$

As (2.6a) and (2.6b) have a unique solution, it is easily established that there exists a unique solution to (3.7). Moreover, the system (3.7) is symmetric and positive definite on $\mathcal{R}_m^\perp$.

Finally, we consider (2.27a)–(2.27c), which can be reformulated as: Find $\{\delta\vec{X}^{m+1}, Y^{m+1}\kappa^{m+1}\} \in (\mathbb{R}^3)^K \times [\mathbb{R}^K]^2$, such that

$$\begin{pmatrix} 0 & \tau_m A_m & -\vec{N}_m^T \\ -M_m & \frac{1}{\xi} A_m + \frac{1}{\alpha} M_m & 0 \\ \vec{N}_m & 0 & \vec{A}_m \end{pmatrix} \begin{pmatrix} \kappa^{m+1} \\ Y^{m+1} \\ \delta\vec{X}^{m+1} \end{pmatrix} = \begin{pmatrix} 0 \\ 0 \\ -\vec{A}_m \vec{X}^m \end{pmatrix}. \tag{3.8}$$

Similarly to (3.5), one can transform (3.8) to

$$Y^{m+1} = \frac{1}{\tau_m} S_m \vec{N}_m^T \delta\vec{X}^{m+1} + \mu 1, \tag{3.9a}$$

$$\kappa^{m+1} = \frac{1}{\tau_m} \left(\frac{1}{\alpha} S_m + \frac{1}{\xi} M_m^{-1}\right) \vec{N}_m^T \delta\vec{X}^{m+1} + \frac{\mu}{\alpha} 1 \tag{3.9b}$$

$$\left(\vec{A}_m + \frac{1}{\tau_m} \vec{N}_m \left[\frac{1}{\alpha} S_m + \frac{1}{\xi} M_m^{-1}\right] \vec{N}_m^T\right) \delta\vec{X}^{m+1} = -\vec{A}_m \vec{X}^m - \frac{\mu}{\alpha} \vec{N}_m 1, \quad (\delta\vec{X}^{m+1})^T \vec{N}_m 1 = 0; \tag{3.9c}$$

where $\mu = \frac{1^T Y^{m+1}}{1^T 1} \in \mathbb{R}$ is unknown. Then (3.9c) is readily replaced by

$$\vec{\Pi}_m \left(\vec{A}_m + \frac{1}{\tau_m} \vec{N}_m \left[\frac{1}{\alpha} S_m + \frac{1}{\xi} M_m^{-1}\right] \vec{N}_m^T\right) \vec{\Pi}_m \delta\vec{X}^{m+1} = -\vec{\Pi}_m \vec{A}_m \vec{X}^m. \tag{3.10}$$

As (2.27a)–(2.27c) has a unique solution, it is easily established that there exists a unique solution to (3.10). Moreover, the system (3.10) is symmetric and positive definite on $\mathcal{R}_m^\perp$.

4. Semidiscrete approximations and tangential motion

Similarly to [7, Remark 2.3], it is worthwhile to consider continuous in time semidiscrete versions of our schemes. For example, we replace (2.6a) and (2.6b) by

$$\langle \vec{X}_{\rm t}, \chi \vec{\nu}^h \rangle^h - \langle \nabla_{\rm s}\kappa, \nabla_{\rm s}\chi \rangle = 0 \quad \forall \chi \in W(\Gamma^h(t)), \tag{4.1a}$$

$$\langle \kappa \vec{\nu}^h, \vec{\eta} \rangle^h + \langle \nabla_{\rm s}\vec{X}, \nabla_{\rm s}\vec{\eta} \rangle = 0 \quad \forall \vec{\eta} \in \underline{V}(\Gamma^h(t)); \tag{4.1b}$$

where we always integrate over the current surface $\Gamma^h(t)$ (with normal $\vec{\nu}^h(t)$) described by the identity function $\vec{X}(t) \in \underline{V}(\Gamma^h(t))$. In addition, $\langle \cdot, \cdot \rangle^{(h)}$ is the same as $\langle \cdot, \cdot \rangle_m^{(h)}$ with Γ^m and $\vec{X}^m$ replaced by $\Gamma^h(t)$ and $\vec{X}(t)$, respectively. It is straightforward to show that (4.1a) and (4.1b) conserves the enclosed volume exactly; since on choosing $\chi = 1$ in (4.1a) and taking into account (2.2) yields that

$$0 = \langle \vec{X}_{\rm t}, \vec{\nu}^h \rangle^h = \int_{\Gamma^h} \vec{X}_{\rm t} \cdot \vec{\nu}^h \,{\rm d}s = \frac{\rm d}{{\rm d}t}[{\rm Vol}(\Gamma^h(t))]. \tag{4.2}$$

To our knowledge, no other direct approximation of (1.2) in the literature satisfies this property. Of course, (4.2) applies to the corresponding semidiscrete analogues of (2.5) with (2.4b), and (2.27a)–(2.27c), as it is based solely on (4.1a) with $\chi = 1$. It does not appear possible to prove the analogue of (4.2) for the fully discrete schemes (2.6a), (2.6b), (2.5) with (2.4b), and (2.27a)–(2.27c). However, in practice we observe that the enclosed volume is approximately preserved, and that the volume loss tends to zero as $\tau \to 0$; see Section 5 for details.

In addition, one can derive a stability bound, the analogue of (2.19), for these semidiscrete approximations. To derive such a result we need the following lemma, which computes the first variation of the area of polyhedral surfaces.

Lemma 4.1. *Let $\Upsilon = \bigcup_{j=1}^J \overline{\sigma}_j$ be a polyhedral surface. Furthermore, let $\vec{Y}^\varepsilon \in \underline{V}(\Upsilon)$, $\varepsilon \in (-\varepsilon_0, \varepsilon_0)$, be parameterizations of polyhedral surfaces which depend smoothly on ε, with $\vec{Y}^0$ being the identity function on Υ. Then we obtain for the polyhedral surfaces $\Upsilon^\varepsilon = \vec{Y}^\varepsilon(\Upsilon)$ that*

$$\frac{\rm d}{{\rm d}\varepsilon}|\Upsilon^\varepsilon||_{\varepsilon=0} = \int_\Upsilon \nabla_{\rm s}\vec{Y}^0 \;\cdot\; \nabla_{\rm s}(\partial_\varepsilon \vec{Y}^\varepsilon|_{\varepsilon=0}) {\rm d}s. \tag{4.3}$$

Proof. Let $\sigma_j(\varepsilon) := \vec{Y}^\varepsilon(\sigma_j)$ and $\{\vec{\rho}_1, \vec{\rho}_2\}$ be an orthonormal basis for the plane containing σ_j. On recalling (2.16), it follows that

$$\begin{aligned}
\frac{\rm d}{{\rm d}\varepsilon}|\sigma_j(\varepsilon)||_{\varepsilon=0} &= \frac{\rm d}{{\rm d}\varepsilon}\int_{\sigma_j} \left|\frac{\partial \vec{Y}^\varepsilon}{\partial \vec{\rho}_1} \times \frac{\partial \vec{Y}^\varepsilon}{\partial \vec{\rho}_2}\right| {\rm d}s|_{\varepsilon=0} = \frac{\rm d}{{\rm d}\varepsilon}\int_{\sigma_j} \left(\left|\frac{\partial \vec{Y}^\varepsilon}{\partial \vec{\rho}_1}\right|^2 \left|\frac{\partial \vec{Y}^\varepsilon}{\partial \vec{\rho}_2}\right|^2 - \left|\frac{\partial \vec{Y}^\varepsilon}{\partial \vec{\rho}_1} \cdot \frac{\partial \vec{Y}^\varepsilon}{\partial \vec{\rho}_2}\right|^2 \right)^{\frac{1}{2}} {\rm d}s|_{\varepsilon=0} \\
&= \int_{\sigma_j} \left(\frac{\partial \vec{Y}^\varepsilon}{\partial \vec{\rho}_1} \cdot \frac{\partial}{\partial \varepsilon}\left[\frac{\partial \vec{Y}^\varepsilon}{\partial \vec{\rho}_1}\right] + \frac{\partial \vec{Y}^\varepsilon}{\partial \vec{\rho}_2} \cdot \frac{\partial}{\partial \varepsilon}\left[\frac{\partial \vec{Y}^\varepsilon}{\partial \vec{\rho}_2}\right] \right) {\rm d}s|_{\varepsilon=0} = \int_{\sigma_j} \nabla_{\rm s}\vec{Y}^0 \cdot \nabla_{\rm s}(\partial_\varepsilon \vec{Y}^\varepsilon|_{\varepsilon=0}) {\rm d}s,
\end{aligned}$$

where we noted that $\frac{\partial \vec{Y}^0}{\partial \vec{\rho}_i}|_{\sigma_j} = \vec{\rho}_i$. Summing over j yields the desired result (4.3). □

Choosing $\chi \equiv \kappa$ in (4.1a) and $\vec{\eta} \equiv \vec{X}_{\rm t}$ in (4.1b) now gives, with the help of Lemma 4.1, that

$$\frac{\rm d}{{\rm d}t}|\Gamma^h(t)| = \int_{\Gamma^h} \nabla_{\rm s}\vec{X} \cdot \nabla_{\rm s}\vec{X}_{\rm t} {\rm d}s = -\int_{\Gamma^h} |\nabla_{\rm s}\kappa|^2 {\rm d}s.$$

Similar stability results can be derived for the other semidiscrete schemes.

In [7, Remark 2.4] and [5, Remark 2.5], we showed for a closed curve that the scheme (4.1a) and (4.1b) for $d = 2$, and the corresponding semidiscrete analogues of (2.4a), (2.4b), (2.5) with (2.4b), and (2.27a)–(2.27c), will always equidistribute the nodes along the polygonal approximation to the curve if the corresponding intervals are not locally parallel. Although it does not appear possible to prove an analogue for the fully discrete schemes, e.g. (2.6a) and (2.6b) for $d = 2$, in practice we saw that the nodes are moved tangentially so that they will eventually be equidistributed. We now investigate the analogue of this result for the present case of a

closed surface in $\mathbb{R}^3$. First, for later purposes, we introduce the following definition. Let $\Upsilon = \bigcup_{j=1}^{J} \overline{\sigma}_j$ be a polyhedral surface and $\vec{Y} \in \underline{V}(\Upsilon)$. Then

$$\underline{V}_{\vec{\tau}}(\Upsilon, \vec{Y}) := \{\vec{\eta} \in \underline{V}(\Upsilon) : \vec{\eta}(\vec{q}_k) \cdot \vec{\omega}_k^{\vec{Y}} = 0, k = 1 \to K\}, \tag{4.4}$$

where $\{\vec{q}_k\}_{k=1}^{K}$ are the vertices of Υ and $\vec{\omega}_k^{\vec{Y}}$ denotes the weighted normal of the polyhedral surface $\vec{Y}(\Upsilon) \subset \mathbb{R}^3$ at the vertex $\vec{Y}(\vec{q}_k)$, $k = 1 \to K$; similarly to (2.7). We set $\underline{V}_{\vec{\tau}}(\Upsilon) := \underline{V}_{\vec{\tau}}(\Upsilon, \vec{\mathrm{id}})$. We then have the following lemma.

Lemma 4.2. *If $\vec{X}_t = \vec{g}$, with $\vec{g}(t,\cdot) \in \underline{V}(\Gamma^h(t))$, then it holds that*

$$\frac{\mathrm{d}}{\mathrm{d}t}[\mathrm{Vol}(\Gamma^h(t))] = 0 \quad \text{if } \vec{g}(t,\cdot) \in \underline{V}_{\vec{\tau}}(\Gamma^h(t)). \tag{4.5}$$

Moreover, if $\vec{X}_t = \vec{g}(t, \vec{q}_k(t))\phi_k$, with $\{\phi_k\}_{k=1}^{K}$ being the standard basis of $\underline{V}(\Gamma^h(t))$, then it holds that

$$\frac{\mathrm{d}}{\mathrm{d}t}[\mathrm{Vol}(\Gamma^h(t))] = 0 \quad \text{if and only if } \vec{g}(t, \vec{q}_k(t)) \cdot \vec{\omega}_k(t) = 0. \tag{4.6}$$

Proof. We have from (4.2) that

$$\frac{\mathrm{d}}{\mathrm{d}t}[\mathrm{Vol}(\Gamma^h(t))] = \langle \vec{X}_t, \vec{\nu}^h \rangle^h = \langle \vec{g}, \vec{\nu}^h \rangle^h = \sum_{k=1}^{K} \vec{g}(t, \vec{q}_k(t)) \cdot \vec{\omega}_k(t) \langle \phi_k, 1 \rangle^h.$$

Hence we obtain (4.5). The remaining result (4.6) can be shown analogously. □

The scheme (4.1a) and (4.1b), and the corresponding semidiscrete analogues of (2.4a), (2.4b), (2.5) with (2.4b), and (2.27a)–(2.27c), will always distribute the vertices on $\Gamma^h(t)$ according to a criterion, which is based solely on (4.1b). We now investigate this criterion.

For any fixed $t > 0$, we consider variations of $\Gamma^h(t)$ which are of the form $\vec{Y}^\varepsilon : \Gamma^h(t) \to \mathbb{R}^3$ such that $\vec{Y}^\varepsilon \in \underline{V}(\Gamma^h(t))$; and hence yield a polyhedral surface Υ^ε, which we assume to be non-degenerate. In addition, we assume that $\vec{Y}^\varepsilon$ is smooth in ε, $\vec{Y}^0 = \vec{\mathrm{id}}$ and $\partial_\varepsilon \vec{Y}^\varepsilon|_{\varepsilon=0} \in \underline{V}_{\vec{\tau}}(\Gamma^h(t))$. As Υ^ε arises from $\Gamma^h(t)$ by variations of the vertices in directions that are tangential to these weighted normals, we obtain from (4.3) and (4.1b) that

$$\frac{\mathrm{d}}{\mathrm{d}\varepsilon}|\Upsilon^\varepsilon||_{\varepsilon=0} = \langle \nabla_s \vec{Y}^0, \nabla_s(\partial_\varepsilon \vec{Y}^\varepsilon|_{\varepsilon=0}) \rangle \equiv \langle \nabla_s \vec{X}, \nabla_s(\partial_\varepsilon \vec{Y}^\varepsilon|_{\varepsilon=0}) \rangle = -\langle \kappa \vec{\nu}^h, \partial_\varepsilon \vec{Y}^\varepsilon|_{\varepsilon=0} \rangle^h = 0. \tag{4.7}$$

Hence we obtain that infinitesimally small "tangential" changes to $\Gamma^h(t)$ do not decrease its area and, on recalling Lemma 4.2, maintain its volume. Moreover, if we move only one vertex we obtain from (4.6) that the enclosed volume is conserved if and only if this movement is "tangential". Hence no individual vertex in $\Gamma^h(t)$ can be moved so as to maintain the volume, and decrease the area to leading order. An analogous property is true for the corresponding evolution of curves, where we obtain the equidistribution property discussed in [7].

The above shows that $\Gamma^h(t)$ is a critical point of area subject to "tangential" variations. This local criticality condition can be strengthened to a global minimizer on replacing area with the Dirichlet integral. We have on noting (4.4), (4.1b), (2.2) and (2.7) that $\vec{X}(t) \in \underline{V}(\Gamma^h(t))$ is such that

$$\langle \nabla_s \vec{X}, \nabla_s \vec{\eta} \rangle = 0 \quad \forall \vec{\eta} \in \underline{V}_{\vec{\tau}}(\Gamma^h(t)). \tag{4.8}$$

Hence we have, on recalling (2.15), that

$$|\Gamma^h(t)| = \frac{1}{2} \int_{\Gamma^h} |\nabla_s \vec{X}|^2 \mathrm{d}s = \min_{\vec{\eta} \in \underline{V}_{\vec{\tau}}(\Gamma^h(t))} \frac{1}{2} \int_{\Gamma^h} |\nabla_s(\vec{X} + \vec{\eta})|^2 \mathrm{d}s. \tag{4.9}$$

Therefore on recalling (4.5), and similarly to (4.7), we have that the semidiscrete versions of our schemes produce $\vec{X}(t)$ for all $t \in (0, T]$ such that no individual vertex can be moved so as to maintain the volume and at the same time decrease the Dirichlet integral in (4.9). This in practice leads to good mesh properties.

Remark 4.1. We now consider in more detail this redistribution of the vertices discussed above. On recalling (2.7), let $\Lambda_k(t) := \bigcup_{\sigma_j \in \mathcal{T}_k(t)} \overline{\sigma}_j(t)$ be the union of elements meeting at vertex $\vec{q}_k(t)$, and let $\partial\Lambda_k(t)$ have vertices

$\vec{p}_l(t)$, $l = 1 \to L$ with $\vec{p}_{L+1}(t) := \vec{p}_1(t)$, which we assume to be ordered anti-clockwise on the outer surface of $\Lambda_k(t)$. On recalling (2.3), we have that

$$\sum_{\sigma_j \in \mathcal{T}_k} |\sigma_j| \vec{\nu}_j^h = \frac{1}{2} \sum_{l=1}^{L} (\vec{p}_l - \vec{q}_k) \times (\vec{p}_{l+1} - \vec{q}_k) = \frac{1}{2} \sum_{l=1}^{L} \vec{p}_l \times \vec{p}_{l+1}. \tag{4.10}$$

Hence (2.7) and (4.10) imply that the direction of $\vec{\omega}_k(t)$ only depends on the neighbouring points $\{\vec{p}_l(t)\}_{l=1}^L$ and not on $\vec{q}_k(t)$ itself.

We introduce for $l = 1 \to L$

$$\vec{\zeta}_l = \frac{[(\vec{p}_{l+1} - \vec{q}_k) \cdot (\vec{p}_{l+1} - \vec{p}_l)](\vec{p}_l - \vec{q}_k) - [(\vec{p}_l - \vec{q}_k) \cdot (\vec{p}_{l+1} - \vec{p}_l)](\vec{p}_{l+1} - \vec{q}_k)}{|\vec{p}_{l+1} - \vec{p}_l|^2},$$

which is the vector connecting $\vec{q}_k$ to the line through $\vec{p}_l$ and $\vec{p}_{l+1}$ so that $\vec{\zeta}_l \cdot (\vec{p}_{l+1} - \vec{p}_l) = 0$, see Fig. 1. It follows that

$$\int_{\Delta\{\vec{q}_k, \vec{p}_l, \vec{p}_{l+1}\}} \nabla_s \vec{X} \cdot \nabla_s (\vec{z}\phi_k) \mathrm{d}s = -\frac{|\vec{p}_{l+1} - \vec{p}_l|}{2|\vec{\zeta}_l|} \vec{\zeta}_l \cdot \vec{z} \quad \forall \vec{z} \in \mathbb{R}^3. \tag{4.11}$$

Therefore, on choosing $\vec{\eta} = \vec{z}\phi_k$ in (4.1b), and noting (4.11), (2.2) and (2.7), we have that

$$\vec{u}_k := \sum_{l=1}^{L} \frac{|\vec{p}_{l+1} - \vec{p}_l|}{|\vec{\zeta}_l|} \vec{\zeta}_l \in \{\theta \vec{\omega}_k : \theta \in \mathbb{R}\}. \tag{4.12}$$

As $\vec{\omega}_k$ is independent of $\vec{q}_k$, one can view (4.12) as a constraint on $\vec{q}_k$ in terms of its neighbours $\{\vec{p}_l\}_{l=1}^L$.

We now consider the constraint (4.12) in the simple case when the points $\{\vec{p}_l\}_{l=1}^L$ lie in a plane, which we will denote by $\mathcal{P}$. Let $\vec{z}^{\mathcal{P}}$ denote the component of $\vec{z}$ lying in the plane $\mathcal{P}$, then we have that

$$\frac{\vec{\zeta}_l^{\mathcal{P}}}{|\vec{\zeta}_l^{\mathcal{P}}|} = \frac{R_{\mathcal{P}}(\vec{p}_{l+1} - \vec{p}_l)}{|\vec{p}_{l+1} - \vec{p}_l|}, \tag{4.13}$$

where $R_{\mathcal{P}}$ acting on $\mathbb{R}^3$ denotes clockwise rotation by $\frac{\pi}{2}$ in the plane $\mathcal{P}$. It follows from (4.10) that $\vec{\omega}_k$ will be normal to $\mathcal{P}$. Hence, on noting (4.13), we have that (4.12) collapses in this case to

$$\sum_{l=1}^{L} g(|\vec{\zeta}_l^{\mathcal{P}}|)(\vec{p}_{l+1} - \vec{p}_l) = \vec{0} \quad \text{with } g(r) := \frac{r}{(r^2 + |\vec{q}_k - \vec{q}_k^{\mathcal{P}}|^2)^{\frac{1}{2}}}. \tag{4.14}$$

If $\vec{q}_k$ lies in $\mathcal{P}$; that is, Λ_k is flat; then (4.14) is trivially satisfied, with no further constraint on $\vec{q}_k$. This is the surface analogue of locally parallel intervals for curves.

We now examine some non-trivial cases of (4.14), when $\vec{q}_k \notin \mathcal{P}$. (i) If $L = 3$, then on noting that $\vec{p}_1 - \vec{p}_3 = -(\vec{p}_2 - \vec{p}_1) - (\vec{p}_3 - \vec{p}_2)$, $\{\vec{p}_{l+1} - \vec{p}_l\}_{l=1}^2$ are linearly independent and from the strict monotonicity of g it follows that $|\vec{\zeta}_1^{\mathcal{P}}| = |\vec{\zeta}_2^{\mathcal{P}}| = |\vec{\zeta}_3^{\mathcal{P}}|$. Hence $\vec{q}_k^{\mathcal{P}}$ is the centre of the inscribed circle of $\Delta\{\vec{p}_l\}_{l=1}^3$. (ii) If $L = 4$ and $\{\vec{p}_l\}_{l=1}^4$ form a parallelogram, then a similar proof to the above yields that $|\vec{\zeta}_1^{\mathcal{P}}| = |\vec{\zeta}_3^{\mathcal{P}}|$ and $|\vec{\zeta}_2^{\mathcal{P}}| = |\vec{\zeta}_4^{\mathcal{P}}|$; that is, $\vec{q}_k^{\mathcal{P}} = \frac{1}{4}\sum_{l=1}^4 \vec{p}_l$ is the centroid of the parallelogram $\{\vec{p}_l\}_{l=1}^4$. (iii) If $L = 2I$ and $\{\vec{p}_l\}_{l=1}^{2I}$ form a regular $2I$

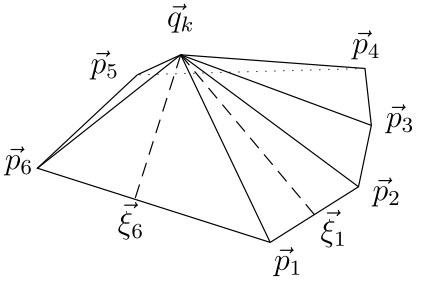

Fig. 1. Sketch of Λ_k and $\{\vec{p}_l\}_{l=1}^L$ for $L = 6$.

polygon, we can choose a local coordinate system so that $\vec{p}_l$ has components $\rho(\cos\gamma_l, \sin\gamma_l, 0)$ with $\gamma_l = \frac{(l-j)\pi}{I}$ for some fixed integer $j \in [1, 2I]$ and some $\rho \in \mathbb{R}_{>0}$. By symmetry, it follows that $|\vec{\zeta}^{\mathcal{P}}_l| + |\vec{\zeta}^{\mathcal{P}}_{l+I}| = 2\rho\cos(\frac{\pi}{4I}) =: c$, $l = 1 \to I$, and so (4.14) yields that

$$\sum_{l=1}^{I} [g(|\vec{\zeta}^{\mathcal{P}}_l|) - g(c - |\vec{\zeta}^{\mathcal{P}}_l|)] \sin\left(\frac{1}{2}[\gamma_l + \gamma_{l+1}]\right) = 0. \tag{4.15}$$

If $\vec{q}^{\mathcal{P}}_k \neq \vec{0}$, the centroid of the parallelogram, then there exists an integer $n \in [1, 2I]$ so that $|\vec{\zeta}^{\mathcal{P}}_l| \geqslant \frac{c}{2}$ for $l = n \to I + n$ with strict inequality for some l, where $\vec{\zeta}^{\mathcal{P}}_l = \vec{\zeta}^{\mathcal{P}}_{l-2I}$ for $l \geqslant 2I + 1$. As $\sin(\frac{1}{2}[\gamma_l + \gamma_{l+1}]) > 0$, for $l = j \to I + j$, we have that (4.15) leads to a contradiction on choosing $j = n$. Hence $\vec{q}^{\mathcal{P}}_k = \frac{1}{2I}\sum_{l=1}^{2I} \vec{p}_l$ is the centroid of the regular polygon $\{\vec{p}_l\}_{l=1}^{2I}$. Therefore we see from this restricted set of examples that (4.12) leads to good mesh properties.

Finally, it does not appear possible to prove the analogue of (4.12) for the fully discrete schemes (2.6a), (2.6b), (2.4a), (2.4b), (2.5) with (2.4b), and (2.27a)–(2.27c). However, in practice we see that the vertices are moved tangentially so that they will eventually satisfy (4.12) up to a tolerance. In particular, all the computations for our fully discrete schemes in this paper could be performed without heuristically redistributing the mesh points, see Section 5 for details.

4.1. Conformal polyhedral surfaces

We now return to the fully discrete case. It turns out that in a certain sense the parameterization $\vec{X}^{m+1} : \Gamma^m \to \Gamma^{m+1}$ can be interpreted as a discrete conformal parameterization. We recall that in the smooth case a conformal parameterization of a surface can be characterized as a parameterization which minimizes the Dirichlet integral in the class of all parameterizations of the same surface, see e.g. [22]. In this variational characterization, the degrees of freedom are given by the reparameterizations, i.e. one uses the tangential degrees of freedom in the parameterization. This idea can be extended to the polyhedral case. Now the degrees of freedom are given by movements of the vertices $\vec{q}^m_k$ in directions orthogonal to the corresponding weighted normals $\vec{\omega}^m_k$. Hence we define a discrete conformal map (parameterization) as follows.

Let Υ and Γ be two polyhedral surfaces, which allow for a continuous piecewise linear parameterization $\vec{Y} : \Upsilon \to \Gamma$. We call $\vec{Y} \in \underline{V}(\Upsilon)$ *a discrete conformal mapping* if and only if

$$\int_{\Upsilon} |\nabla_s \vec{Y}|^2 \mathrm{d}s = \min_{\vec{\eta} \in \underline{V}_{\vec{\tau}}(\Upsilon, \vec{Y})} \int_{\Upsilon} |\nabla_s(\vec{Y} + \vec{\eta})|^2 \mathrm{d}s, \tag{4.16}$$

where we recall the definition (4.4). In addition, we call Υ a *conformal polyhedral surface* if and only if $\vec{\mathrm{id}} : \Upsilon \to \Upsilon$ is a discrete conformal mapping. Similarly to (4.8), taking the first variation of the Dirichlet energy for a discrete conformal map $\vec{Y}$ yields that

$$\int_{\Upsilon} \nabla_s \vec{Y} \cdot \nabla_s \vec{\eta} \mathrm{d}s = 0 \quad \forall \vec{\eta} \in \underline{V}_{\vec{\tau}}(\Upsilon, \vec{Y}).$$

In the case of smooth surfaces Υ and Γ, a conformal mapping $\vec{Y} : \Upsilon \to \Gamma$ has the property that $\Delta_s \vec{Y}$ is normal to $\vec{Y}(\Upsilon)$, see e.g. [22]. Given a polyhedral surface Υ, we define the discrete Laplace–Beltrami operator on Υ, $\Delta^h_s : \underline{V}(\Upsilon) \to \underline{V}(\Upsilon)$, such that for any $\vec{Z} \in \underline{V}(\Upsilon)$

$$\langle \Delta^h_s \vec{Z}, \vec{\eta} \rangle^h_{\Upsilon} = -\langle \nabla_s \vec{Z}, \nabla_s \vec{\eta} \rangle_{\Upsilon} \quad \forall \vec{\eta} \in \underline{V}(\Upsilon), \tag{4.17}$$

where $\langle \cdot, \cdot \rangle_{\Upsilon}$ and $\langle \cdot, \cdot \rangle^h_{\Upsilon}$ are the Υ analogues of $\langle \cdot, \cdot \rangle_m$ and $\langle \cdot, \cdot \rangle^h_m$ over Γ^m. On noting (1.1), one can interpret $\Delta^h_s \vec{\mathrm{id}}$ as a discrete mean curvature vector for the polyhedral surface Υ. For a discrete conformal mapping $\vec{Y} : \Upsilon \to \Gamma$, it follows that $\Delta^h_s \vec{Y}(\vec{q}_k)$ lies in the direction of $\vec{\omega}^{\vec{Y}}_k$ for all k, where $\vec{q}_k$ are the vertices of Υ and $\vec{\omega}^{\vec{Y}}_k$ are the weighted normals of the polyhedral surface $\vec{Y}(\Upsilon)$. In general the directions of steepest descent of area and volume give two competing notions of a normal vector at a vertex, see [27, p. 3]. On recalling Lemmas 4.1 and 4.2, we observe that for a conformal polyhedral surface these two notions collapse, giving a unique choice for the normal at a vertex.

Remark 4.2. Our definition (4.16) is in agreement with the definition of discrete conformal maps by [11]. These authors do not state the orthogonality condition explicitly, as they consider only the case where $\Gamma \subset \mathbb{R}^2 \cong \mathbb{R}^2 \times \{0\}$. In this case $\vec{\omega} = (0,0,1)^T$, which allows for movement of the vertices only in the (x_1, x_2)-plane. This means that they compute a mapping between a discrete surface and a planar mesh. The definition given in (4.16) is of course more general.

In addition, using the standard cotangent formula for the element stiffness matrix of the Dirichlet integral, one can rewrite the Dirichlet energy in (4.16) in terms of the cotangents of the angles of the polyhedral surface Υ and the length of the edges on Γ, see e.g. [24,11].

Let Γ^m and Γ^{m+1} be the polyhedral surfaces generated from (2.6a) and (2.6b), or the schemes (2.4a), (2.4b), (2.5) with (2.4b), and (2.27a)–(2.27c). We obtain from (2.6b), and its analogues, that

$$\int_{\Gamma^m} \nabla_s \vec{X}^{m+1} \cdot \nabla_s \vec{\eta} \, \mathrm{d}s = 0 \quad \forall \vec{\eta} \in \underline{V}_{\vec{\tau}}(\Gamma^m, \vec{X}^m). \tag{4.18}$$

This implies that in some sense $\vec{X}^{m+1} : \Gamma^m \to \Gamma^{m+1}$ is an approximate discrete conformal map as, in contrast to (4.16), the orthogonality constraints are imposed explicitly on Γ^m. Note that it follows from (4.9) that for the semidiscrete versions of our schemes, e.g. (4.1a) and (4.1b), we have that at any time $t > 0$, $\Gamma^h(t)$ is a conformal polyhedral surface.

Remark 4.3. Given a polyhedral surface Γ^0, an approach to compute a conformal polyhedral surface close to Γ^0 could be to consider the natural generalization of our fully discrete schemes to the trivial evolution equation

$$\mathcal{V} = \vec{x}_t \cdot \vec{\nu} = 0, \tag{4.19}$$

see also [7, Remark 2.4]. Similarly to e.g. (2.6a) and (2.6b), the approximation would be: Find $\{\vec{X}^{m+1}, \kappa^{m+1}\} \in \underline{V}(\Gamma^m) \times W(\Gamma^m)$ such that

$$\langle \vec{X}^{m+1} - \vec{X}^m, \chi \vec{\nu}^m \rangle^h_m = 0 \quad \forall \chi \in W(\Gamma^m), \tag{4.20a}$$

$$\langle \kappa^{m+1} \vec{\nu}^m, \vec{\eta} \rangle^h_m + \langle \nabla_s \vec{X}^{m+1}, \nabla_s \vec{\eta} \rangle_m = 0 \quad \forall \vec{\eta} \in \underline{V}(\Gamma^m). \tag{4.20b}$$

Of course, in this case it is possible to eliminate κ^{m+1} from (4.20a) and (4.20b). Then one obtains a symmetric positive semi-definite system for the unknowns $\beta_i^{m+1} \in W(\Gamma^m)$, $i = 1 \to 2$, where $\vec{X}^{m+1}(\vec{q}_k^m) = \vec{X}^m(\vec{q}_k^m) + \sum_{i=1}^2 [\beta_i^{m+1}]_k \vec{\tau}_{i,k}^m$, $k = 1 \to K$, and for each k $\{\vec{\omega}_k^m, \vec{\tau}_{1,k}^m, \vec{\tau}_{2,k}^m\}$ form an orthogonal basis of $\mathbb{R}^3$. In particular, it is then straightforward to show that $\vec{X}^{m+1} = \vec{X}^m$ solves (4.20a) and (4.20b) if and only if $\vec{X}^m$ satisfies (4.12) for all k. Moreover, in practice we observe that the scheme (4.20a) and (4.20b) moves the vertices such that, after a number of steps, they eventually satisfy (4.12) up to a tolerance. This suggests that in practical computations the scheme can be used as a natural redistribution step that approximately preserves volume, recall (4.5). However, since the approximations (2.4a), (2.4b), (2.5) with (2.4b), (2.6a), (2.6b) and (2.27a)–(2.27c) intrinsically incorporate an analogous tangential velocity, we did not employ the scheme (4.20a) and (4.20b) for our computations. Furthermore, it is not clear under which conditions the scheme (4.20a) and (4.20b) produces "nice" meshes, in particular for very non-uniform initial triangulations, and this open question needs further research. Finally, note that the natural extensions of the schemes (2.24) and (2.26a)–(2.26d) to approximate (4.19) would not change the initial parameterization $\vec{X}^0$.

5. Numerical simulations

In this section we first state some information on how we solved the discrete equations and then present several numerical computations.

The Schur complement systems (3.3b), (3.7) and (3.10) can be easily solved with a conjugate gradient solver. Where necessary, the solution of $A_m y = x$, in order to compute $S_m x$, can be obtained with either a multigrid solver or a preconditioned conjugate gradient solver.

For the Schur system (3.3b) we investigated the following preconditioner $\vec{G}_m \in [\mathbb{R}^{3\times 3}]^{K\times K}$ with diagonal entries

$$[\vec{G}_m]_{ii} = \left[[\vec{A}_m]_{ii} + \frac{1}{\tau_m} [M_m]_{ii}^{-1} \begin{pmatrix} ([\vec{N}_m]_{ii} \cdot \vec{e}_1)^2 & 0 & 0 \\ 0 & ([\vec{N}_m]_{ii} \cdot \vec{e}_2)^2 & 0 \\ 0 & 0 & ([\vec{N}_m]_{ii} \cdot \vec{e}_3)^2 \end{pmatrix} \right]^{-1}, \tag{5.1}$$

where $\vec{e}_i$, $i = 1 \to 3$, are the standard basis vectors in $\mathbb{R}^3$. Employing this preconditioner in practice lead in most cases to only small gains in CPU time. Naturally, the definition (5.1) can easily be adapted to all of the other Schur complement systems. For instance, for the system (3.7) we used the preconditioner

$$\vec{\Pi}_m \vec{H}_m \vec{\Pi}_m \in [\mathbb{R}^{3\times 3}]^{K\times K}, \tag{5.2}$$

where $\vec{H}_m \in [\mathbb{R}^{3\times 3}]^{K\times K}$ is obtained from (5.1) by replacing $[M_m]_{ii}$ with $[A_m]_{ii}$.

The same idea can also be applied to the approximation (2.26a)–(2.26d). Recall that the Schur complement system for (2.26a)–(2.26d) as stated in [4] can be written as

$$\Pi_m \left(\tau_m \vec{\mathcal{N}}_m^T \vec{\mathcal{M}}_m^{-1} \vec{A}_m \vec{\mathcal{M}}_m^{-1} \vec{\mathcal{N}}_m + \mathcal{M}_m S_m \mathcal{M}_m \right) \Pi_m V^{m+1} = -\Pi_m \vec{\mathcal{N}}_m^T \vec{\mathcal{M}}_m^{-1} \vec{A}_m \vec{X}^m, \tag{5.3a}$$

$$\vec{V}^{m+1} = \vec{\mathcal{M}}_m^{-1} \vec{\mathcal{N}}_m V^{m+1}, \tag{5.3b}$$

where $\mathcal{M}_m$ and $\vec{\mathcal{N}}_m$ are the non-lumped versions of M_m and $\vec{N}_m$, $\vec{\mathcal{M}}_m$ derives from $\mathcal{M}_m$ in the obvious fashion, and $\Pi_m := Id_K - \frac{ww^T}{w^T w}$, where $w := \mathcal{M}_m 1$ is the orthogonal projection onto $(\mathrm{span} w)^\perp$. The natural extension of the preconditioner (5.1) to (5.3a) is $\Pi \mathcal{H}_m \Pi$, where the entries of the diagonal operator $\mathcal{H}_m$ are given by

$$[\mathcal{H}_m]_{ii} = \left[\tau_m [\mathcal{M}_m]_{ii}^{-2} [A_m]_{ii} ([\vec{\mathcal{N}}_m]_{ii} \cdot [\vec{\mathcal{N}}_m]_{ii}) + [\mathcal{M}_m]_{ii}^2 [A_m]_{ii}^{-1} \right]^{-1}. \tag{5.4}$$

The system (3.4b) can be solved with an inexact Newton method. When f is given by (1.6), because of the singularity of $f^{-1} = f$ at the origin, the discrete system (3.4b) needs to be solved with a damped inexact Newton method, where as initial guess for the Newton iteration we choose $\delta \vec{X}^{m+1,0} := \vec{N}_m 1$. Moreover, we only perform computations for (2.4a), (2.4b) with (1.6), where the evolution is initially well defined, e.g. where the initial data $\vec{x}(\cdot, 0)$ is such that that $\varkappa(\cdot, 0) < 0$. In practice, the damped Newton method always converged in these cases and we always observed that $\kappa^m < 0$, $m = 1 \to M$. For the scheme (2.5) with (2.4b) we set $\kappa^0 := -(\vec{N}_0{}^T \vec{N}_0)^{-1} \vec{N}_0{}^T \vec{A}_0 \vec{X}^0$, on noting that $\vec{N}_0{}^T \vec{N}_0$ is a diagonal matrix with strictly positive diagonal entries.

Throughout the majority of this section we use (almost) uniform time steps; in that, $\tau_m = \tau$, $m = 0 \to M-2$, and $\tau_{M-1} = T - t_{m-1} \leqslant \tau$. For later purposes, we define

$$\vec{X}(t) := \frac{t - t_{m-1}}{\tau_m} \vec{X}^m + \frac{t_m - t}{\tau_{m-1}} \vec{X}^{m-1}, \quad t \in [t_{m-1}, t_m] \quad m \geqslant 1.$$

On recalling (2.7), we set

$$h_{\vec{X}^m} := \max_{k=1\to K} \left\{ \max_{\vec{p}_l \in \partial \Lambda_k^m} |\vec{X}^m(\vec{q}_k^m) - \vec{X}^m(\vec{p}_l)| \right\} \quad \text{and} \quad \ell_{\vec{X}^m} := \min_{k=1\to K} \left\{ \min_{\vec{p}_l \in \partial \Lambda_k^m} |\vec{X}^m(\vec{q}_k^m) - \vec{X}^m(\vec{p}_l)| \right\}.$$

Finally, we note that we implemented the approximations within the finite element toolbox ALBERTA, see [26].

5.1. Mean curvature flow

First, we compare our scheme (2.4a) and (2.4b) with $f(r) := r$, i.e. (2.25), with another algorithm in the literature, namely the scheme (2.24) from [12]. As a first test, we performed the following convergence test for a true solution. An exact solution to (1.7) with $f(r) := r$, so that the resulting $\Gamma(t)$ solves (1.3), is given by

$$\vec{x}(\cdot, t) = (1 - 4t)^{\frac{1}{2}} \vec{\mathrm{id}}_{S^2}, \quad \varkappa(\cdot, t) = -2(1 - 4t)^{-\frac{1}{2}}, \quad t \in [0, \overline{T}), \quad \overline{T} = \frac{1}{4}, \tag{5.5}$$

where $\vec{\mathrm{id}}_{S^2}$ is the identity function on the unit sphere $\Omega \equiv S^2 \subset \mathbb{R}^3$. We note that $\vec{x}_t = (\vec{x}_t \cdot \vec{\nu})\vec{\nu}$ for the solution (5.5). We compare our results from (2.25) to the scheme (2.24), see Table 1. We used $\tau = 0.125 h_{\vec{X}^0}^2$ and either $T = \frac{1}{2}\overline{T}$ or $T = \overline{T} - \tau$. Here and in what follows we always compute the error $\|\vec{X} - \vec{x}\|_{L^\infty} := \max_{m=1\to M} \|\vec{X}(t_m)$

Table 1
Absolute errors $\|\vec{X} - \vec{x}\|_{L^\infty}$ for the test problem, with $T = \frac{1}{2}\overline{T} = \frac{1}{8}$ and $T = \overline{T} - \tau$, respectively

K	$h_{\vec{X}^0}$	(2.24)		(2.25)	
		$T = \frac{1}{2}\overline{T}$	$T = \overline{T} - \tau$	$T = \frac{1}{2}\overline{T}$	$T = \overline{T} - \tau$
50	7.6537e−01	8.1912e−02	1.3737e−01	5.0141e−02	8.9682e−02
194	4.0994e−01	3.2520e−02	1.4146e−01	2.2436e−02	1.1659e−01
770	2.0854e−01	9.4537e−03	1.0740e−01	6.6398e−03	9.5429e−02
3074	1.0472e−01	2.4838e−03	7.0331e−02	1.7573e−03	6.4653e−02
12,290	5.2416e−02	6.3764e−04	4.3437e−02	4.5446e−04	4.0813e−02
49,154	2.6215e−02	1.6224e−04	2.5388e−02	1.1635e−04	2.4156e−02

$-\vec{x}(\cdot, t_m)\|_{L^\infty}$, where $\|\vec{X}(t_m) - \vec{x}(\cdot, t_m)\|_{L^\infty} := \max_{k=1\to K}\{\min_{\vec{y}\in\Omega}|\vec{X}^m(\vec{q}^m_k) - \vec{x}(\vec{y}, t_m)|\}$ between $\vec{X}$ and the true solution on the interval $[0, T]$. We note that the experiments indicate that the convergence rate for the error away from the singularity is $O(h^2)$, and up to the singularity at time $\overline{T}$ is of order less than $O(h)$, for both schemes; as one may expect.

The next experiment is for a $2 \times 1 \times 1$ cuboid. The initial triangulation is given by $K = 1282$ vertices and $J = 2560$ triangles. The remaining parameters are chosen as $\tau = 10^{-3}$ and $T = 0.14$. In order to highlight one difference between the two schemes in consideration, we plot for each of them the ratios

$$r_h := h_{\vec{X}^m}/\ell_{\vec{X}^m} \quad \text{and} \quad r_a := \max_{j=1\to J}|\sigma^m_j| / \min_{j=1\to J}|\sigma^m_j|$$

over time, see Fig. 3. The evolution of the two schemes can be seen in Fig. 2. One can clearly see that the ratios increase substantially for scheme (2.24), while the tangential movement of vertices induced by our scheme, as discussed in Section 4, results in only a moderate increase in the ratios r_h and r_a. In order to underline this point further, we conducted an experiment for area preserving mean curvature flow, (1.8). The initial surface for our approximation (2.5), with $f(r) := r$, and (2.4b) consists of a unit cube, where the parameterization is such that it is very coarse for the lower part, and reasonably fine for the upper part. We used the parameters $K = 442$, $J = 880$, $T = 1$ and $\tau = 10^{-3}$. In Fig. 4 we show $\vec{X}(t)$ at different times. The relative volume loss for this computation was -0.86%.

Next we study the possible evolutions of a torus under mean curvature flow, where the torus is given by the equation $(R - \sqrt{x_1^2 + x_2^2})^2 + x_3^2 = r^2$. Here, depending on the ratio of the torus's radii $R > 0$ and $r \in (0, R)$, the torus will either merge to a disk or it will shrink to a circle. In Fig. 5 we plot the surface above, and the corresponding cross-section below, of an example of the former case with $R = 1$ and $r = 0.7$; while in Fig. 6 an example for a shrinking torus with $R = 1$ and $r = 0.5$ is given. The discretization parameters are $K = 1024$, $J = 2048$ and $\tau = 10^{-3}$ with $T = 0.09$ or $T = 0.138$, respectively. We note that the evolution in Fig. 5 shows the onset of a change in topology. Of course, our parametric approximation cannot compute beyond that singularity.

For the first experiment for the nonlinear approximation (2.4a) and (2.4b) we used the exact solution to (1.4) with (1.5):

$$\vec{x}(\cdot, t) = (1 - 2^\beta(\beta+1)t)^{\frac{1}{\beta+1}}\vec{\mathrm{id}}_{S^2}, \quad \varkappa(\cdot, t) = -2(1 - 2^\beta(\beta+1)t)^{-\frac{1}{\beta+1}}, \quad t \in [0, \overline{T}),$$

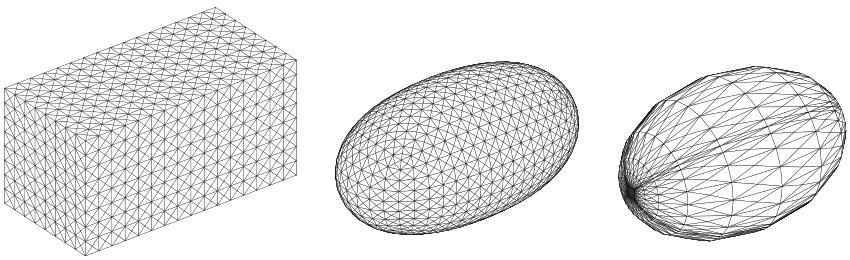

Fig. 2. A plot of $\vec{X}(t)$ at times $t = 0, T = 0.14$ (scaled). On the right $\vec{X}(T)$ for scheme (2.24).

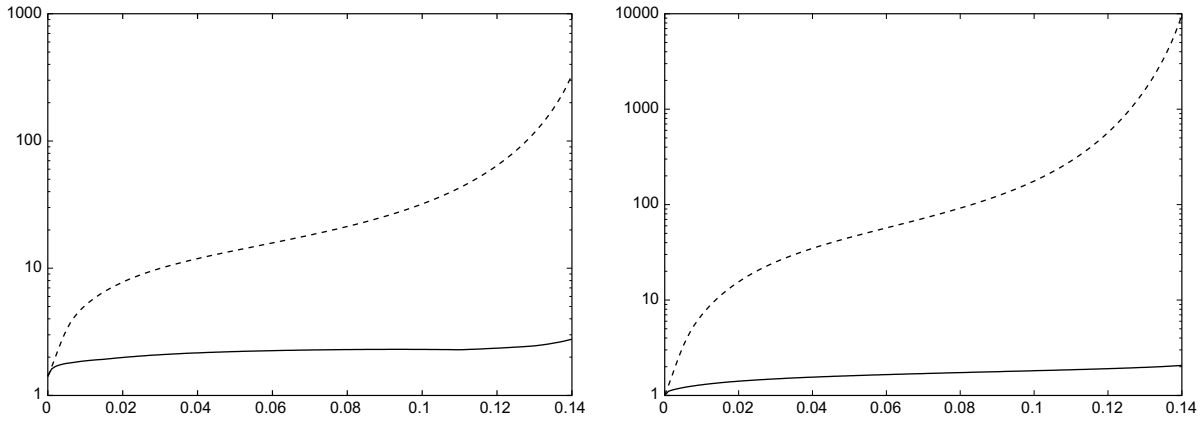

Fig. 3. Plots of $\log r_h$ and $\log r_a$ for the two schemes (2.24) [dashed], and (2.25) [solid].

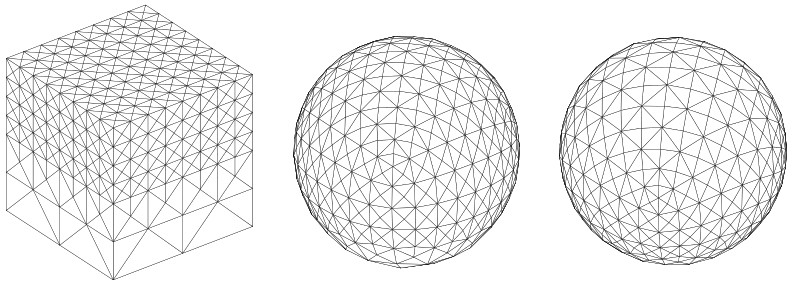

Fig. 4. Plots of $\vec{X}(t)$ at times $t = 0, 0.1, T = 1$.

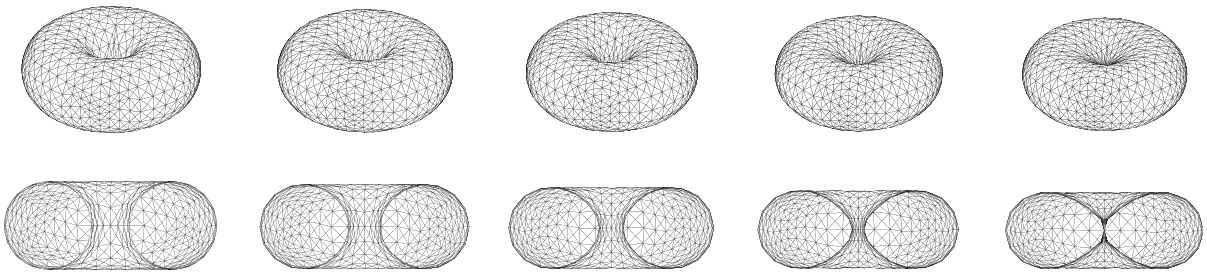

Fig. 5. Plots of $\vec{X}(t)$ at times $t = 0, 0.025, 0.05, 0.075,\ T = 0.09$.

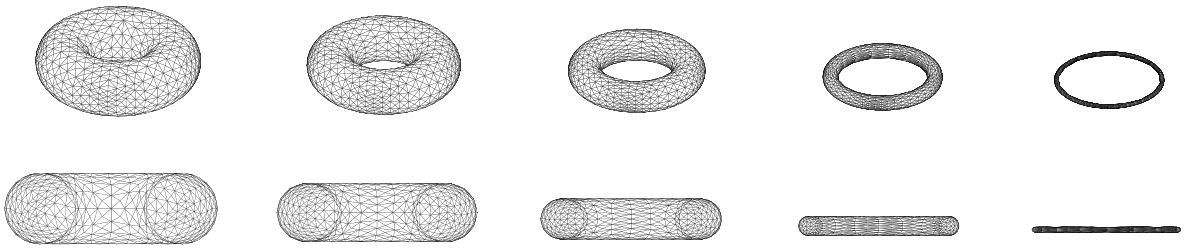

Fig. 6. Plots of $\vec{X}(t)$ at times $t = 0, 0.05, 0.1, 0.13,\ T = 0.138$.

where $\overline{T} = 2^{-\beta}(\beta+1)^{-1}$ and $\Omega = S^2$ is the reference manifold as in (5.5). We note once again that here $\vec{x}_t = (\vec{x}_t \cdot \vec{v})\vec{v}$. We report on a corresponding error table for $\beta = \frac{1}{2}$ and $\beta = \frac{1}{3}$ in Table 2, where we used $\tau = 0.125 h^2_{\vec{X}^0}$. The errors indicate the same convergence rates as in Table 1.

5.2. Inverse mean curvature flow

Here we consider the flow (1.4) with (1.6). First, we performed a convergence test for the approximation (2.4a) and (2.4b) with f given by (1.6). A true solution to (1.7) and (1.6), with $\vec{x}_t = (\vec{x}_t.\vec{v})\vec{v}$, is given by

$$\vec{x}(\cdot,t) = \exp(\frac{t}{2})\vec{\mathrm{id}}_{S^2}, \quad \varkappa(\cdot,t) = -2\exp(-\frac{t}{2}), \quad (t \in 0,\infty),$$

where $\Omega = S^2$ as in (5.5). We report on the corresponding errors for $\tau = 0.125 h^2_{\vec{X}^0}$ in Table 3. The next experiment is for a 3:1:1 ellipsoid with unit semiminor axis that expands to a sphere. The discretization parameters are $K = 1282$, $J = 2560$, $\tau = 10^{-3}$ and $T = 3$, see Fig. 7.

In contrast to curves in $\mathbb{R}^2$, for hypersurfaces in $\mathbb{R}^3$ it is possible to start the classical inverse mean curvature flow with a non-convex initial condition; e.g. for a thin torus with $\varkappa(\cdot,0) < 0$. Here the classical flow by inverse

Table 2
Absolute errors $\|\vec{X} - \vec{x}\|_{L^\infty}$ for the test problem, with $T = \frac{1}{2}\overline{T}$ and $T = \overline{T} - \tau$, respectively

K	$h_{\vec{X}^0}$	$\beta = \frac{1}{2}$		$\beta = \frac{1}{3}$	
		$T = \frac{1}{2}\overline{T}$	$T = \overline{T} - \tau$	$T = \frac{1}{2}\overline{T}$	$T = \overline{T} - \tau$
50	7.6537e−01	1.7291e−02	5.2587e−02	2.2824e−02	2.4162e−02
194	4.0994e−01	7.7622e−03	5.5214e−02	6.6062e−03	2.8945e−02
770	2.0854e−01	2.3182e−03	3.7071e−02	2.0092e−03	1.8502e−02
3074	1.0472e−01	6.3384e−04	2.0660e−02	6.0086e−04	9.4968e−03
12,290	5.2416e−02	1.6782e−04	1.0370e−02	1.7430e−04	4.3659e−03

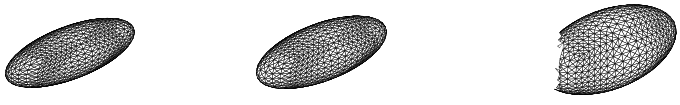

me
an
T =
me
inc
an
κ^m
cha
to
t =
fac
by

We
$\kappa_\star$(

5.3.

V
pare
tion
with

16,29], only exists for a finite time. As an example we take a torus with large radius $R = 1$ 0.25. The discretization parameters are $K = 4096$, $J = 8192$ and $\tau = 5 \times 10^{-4}$ with t the evolution shown in Fig. 8 is only physical as long as the classical flow by inverse The classical flow encounters a singularity once the small radius of the torus has o result in regions with non-negative mean curvature. However, solving for (3.4a) d a Newton method, as described above, always results in approximations with algorithm simply integrates over that singularity until it encounters a topological ıot clear what motion we approximate after times when the classical solution ceases results suggest that for the evolution given in Fig. 8 this happens at around time s estimate by monitoring the approximate mean curvature $\kappa^m_\star$ of the polyhedral sur- a sign change. Here, on recalling (1.1), (4.17) and Remark 2.1, $\kappa^m_\star \in W(\Gamma^m)$ is given $k = 1 \to K$, where $\vec{\kappa}^m \in \underline{V}(\Gamma^m)$ is such that

$$\langle {}^{7}{}_{s}\vec{\eta} \rangle_m \quad \forall \vec{\eta} \in \underline{V}(\Gamma^m).$$

g in the definition of $\kappa^m_\star$ is motivated by the fact that, on noting e.g. (2.4b), $\vec{\kappa}^m(\vec{q}^m_k)$.

t for the unit cube, that evolves to a sphere with the same volume. Here we com-) and (2.6b) with the scheme (2.26a)–(2.26d) from [4]. The initial parameteriza- by $J = 3072$ triangles and $K = 1538$ vertices and the time step size is $\tau = 10^{-4}$ the evolution for both schemes in Figs. 9 and 10, respectively. While our

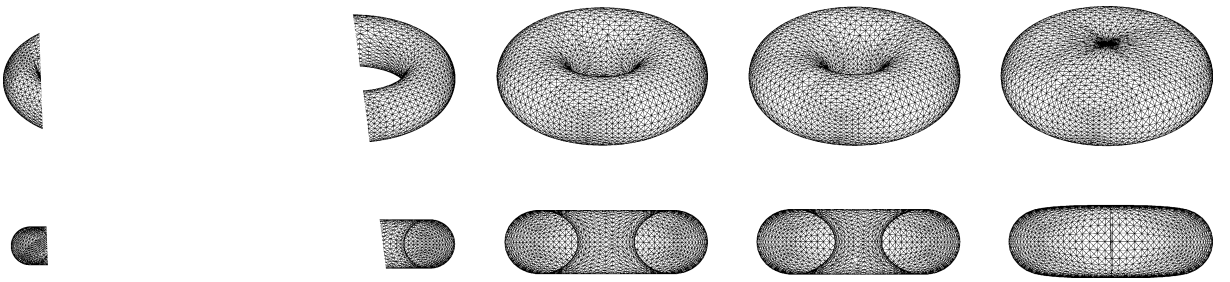

Plots of $\vec{X}(t)$ at times $t = 0, 0.25, 0.5, 0.52,\ T = 0.54$.

scheme can integrate this example without difficulty, we note that due to the lack of tangential movement, the latter approximation develops "ears" that are purely numerical artifacts. Moreover, the linear system that needs to be solved at each time level gets more and more ill-conditioned, which means that eventually the algorithm cannot integrate any further. The overall CPU time for the scheme (2.26a)–(2.26d) for this computation is 105 s, while our the scheme (2.6a) and (2.6b) needs only 9 s (with or without the preconditioner (5.2)). Note that when the preconditioner (5.4) is employed, the computation time for the scheme (2.26a)–(2.26d) reduces to 75 s. This is due to the maximal iteration number being reduced from 92 to 54.

We now want to investigate the character and the effect of the tangential movement induced by our the scheme (2.6a) and (2.6b), as discussed in Section 4, further. Firstly, we investigate how an initial parameterization of the unit sphere is changed in time by our approximation (2.6a) and (2.6b). We compare this evolution to the purely tangential redistribution resulting from the scheme (4.20a) and (4.20b) with the same number of "time steps". The initial parameterization is given by $J = 768$ triangles and $K = 386$ vertices, while $\tau = 10^{-3}$ and $T = 10$. The evolution of the mesh for our approximation (2.6a) and (2.6b) can be seen in Fig. 11, while we omit the evolution for (4.20a) and (4.20b) as it looks very similar. The absolute volume losses for these experiments were 2.5×10^{-5} and -5.6×10^{-6}, respectively. On recalling (4.12), we also monitor the quantity

$$\mathrm{d}(t_m) := \left(\sum_{k=1}^{K} \min_{\theta \in \mathbb{R}} |\vec{u}_k^m - \theta \vec{\omega}_k^m|^2 \right)^{\frac{1}{2}}$$

over time. A plot of $\log \mathrm{d}$ for both of the schemes (2.6a), (2.6b) and (4.20a), (4.20b) is given in Fig. 12. We can clearly see that during the evolution $\mathrm{d}(t)$ is steadily decreased so that the final mesh satisfies the criterion (4.12) up to a tolerance. We also note that this decrease is much faster for the scheme (4.20a) and (4.20b), as there is no normal movement of mesh points. Moreover, we note that the final triangulation in Fig. 11 exhibits many

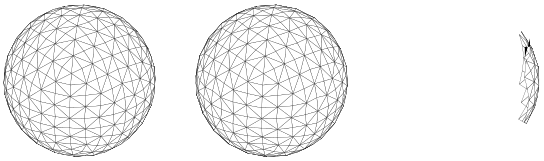

groups of two, four and eight triangles that form "curved squares". We remark that no other scheme published in the literature does intrinsically move the mesh points so that no coalescence of mesh points or other mesh distortion occur in practice.

In order to cure the non-physical mesh distortions produced by the scheme (2.26a)–(2.26d), the authors in [4] consider a heuristical mesh regularization that needs to be applied after each time step. For instance, for the computation in Fig. 10 this leads to the evolution shown in Fig. 13.

Furthermore, we perform the following convergence test for our the scheme (2.6a) and (2.6b). As initial shape we choose a 3:1:1 ellipsoid with unit semiminor axis, and let $\tau = 0.125 h_{\vec{X}^0}^2$ with $T = 50$, by which time the numerical solutions have reached a spherical "steady state". In Table 4 we report on the relative volume loss compared to the volume $V^0 = \mathrm{Vol}(\Gamma^0)$ of the initial polyhedral surface Γ^0, as well as the error $|V^M - V(0)| \equiv |\mathrm{Vol}(\Gamma^M) - \mathrm{Vol}(\Gamma(0))|$ and the indicative error $||\Gamma^M| - \lim_{t\to\infty}|\Gamma(t)||$, i.e. the differences in volume and in surface area to the true asymptotic solution $\vec{x}^\star := \lim_{t\to\infty}\vec{x}(\cdot,t)$, which is given by a sphere. We also report on the error $\|\vec{X}(T) - \vec{x}^\star\|_{L^\infty}$ between $\vec{X}(T)$ and the true asymptotic solution $\vec{x}^\star$.

The evolution of a torus under surface diffusion leads to a change of topology. To demonstrate this, we start the evolution with a torus with radii $R = 1$ and $r = 0.25$, and used discretization parameters $K = 1024$, $J = 2048$, $\tau = 10^{-4}$ and $T = 0.025$. The results are shown in Fig. 14, where we note once again that our parametric approximation cannot compute beyond the topological change. Similarly, we show the evolution of a "cage" under surface diffusion in Fig. 15. The dimensions of the initial surface are $4 \times 4 \times 4$, with the region enclosed by Γ^0 given as the union of 12 cuboids of dimension $4 \times 1 \times 1$. Here a topological change is encountered when the six holes of the surface are about to close to form a hollow ball. The discretization

Table 4
Relative volume loss and some errors with respect to the true asymptotic solution $\vec{x}^\star := \lim_{t\to\infty}\vec{x}(\cdot,t)$

K	$h_{\vec{X}^0}$	$\frac{\lvert V^0 - V^M\rvert}{\lvert V^0\rvert}$	$\lvert V^M - V(0)\rvert$	$\lvert\lvert\Gamma^M\rvert - \lim_{t\to\infty}\lvert\Gamma(t)\rvert\rvert$	$\|\vec{X}(T) - \vec{x}^\star\|_{L^\infty}$
16	1.9467e−00	6.3%	6.9811e−00	9.5912e−00	3.3203e−01
58	1.5081e−00	4.15%	2.5483e−00	3.2503e−00	9.9170e−02
226	9.9812e−01	2.64%	9.0187e−01	1.1542e−00	3.4536e−02
898	5.5384e−01	1.14%	2.9220e−01	3.7802e−01	1.1281e−02
3586	2.8926e−01	0.38%	8.5051e−02	1.1081e−01	3.3158e−03
14,338	1.4752e−01	0.11%	2.3124e−02	3.0255e−02	9.0979e−04

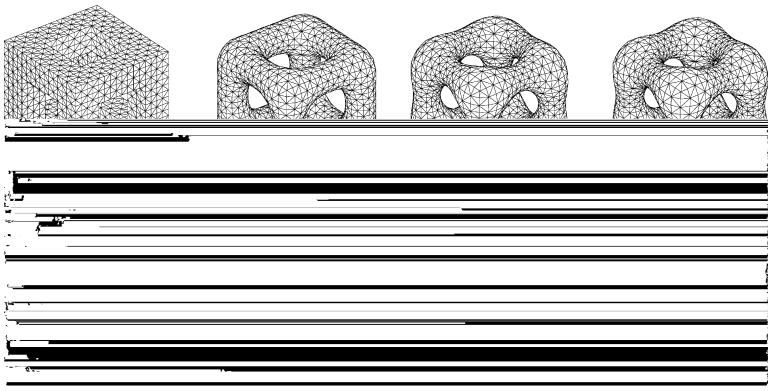

Fig. 15. Plots of $\vec{X}(t)$ at times $t = 0, 0.01, 0.05, 0.1, 0.2, 0.3, 0.4,\ T = 0.48$.

parameters were chosen to be $K = 1912$, $J = 3840$, $\tau = 5 \times 10^{-4}$ and $T = 0.48$. The observed relative volume loss was 1.04%.

The next experiment shows the evolution of a $4 \times 1 \times 1$ cuboid. As discretization parameters we chose $K = 1154$ vertices and $J = 2304$ triangles, with $\tau = 10^{-4}$ and $T = 0.5$. The evolution is shown in Fig. 16, where we once again observe that the induced tangential movement of vertices leads to nice mesh properties throughout the evolution. The relative volume loss for this experiment was 1.55%.

5.4. Intermediate evolution laws

In this subsection, we report on numerical results for our approximation (2.27a)–(2.27c) of the intermediate evolution law (1.10). For (1.9) with $\alpha = \xi = 1$ and for an initial surface that is given by a "cigar like" rounded cylinder of dimension $4 \times 1 \times 1$ we used the discretization parameters $K = 1154$, $J = 2304$, $\tau = 10^{-4}$ and $T = 1$. The corresponding results are shown in Fig. 17. The relative volume loss for this experiment was -0.04%. As a comparison, we performed the same experiment for the two geometric evolution laws (1.2) and (1.8) with $f(r) := r$, between which (1.9) interpolates. The results for our approximations (2.6a), (2.6b),

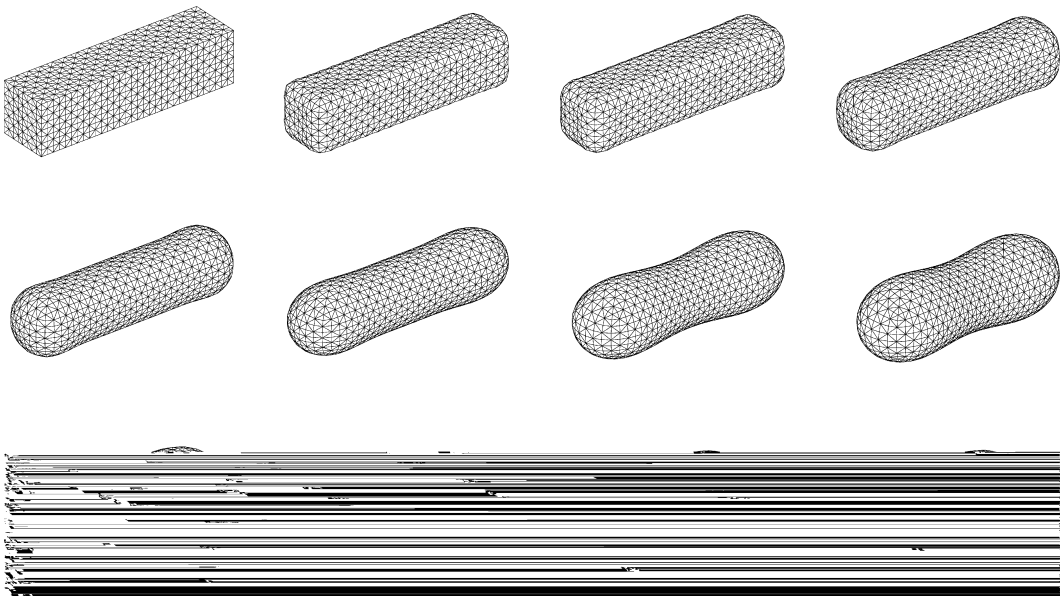

Fig. 16. $\vec{X}(t)$ for $t = 0, 10^{-4}, 2 \times 10^{-4}, 5 \times 10^{-4}, 0.001, 0.005, 0.025, 0.05, 0.1, 0.15, 0.25,\ T = 0.5$.

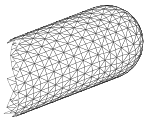

and (2.5), (2.4b), with the same discretization parameters as above, can be seen in Figs. 18 and 19. The relative volume losses for the two computations were 0.02% and −0.02%, respectively. We note the qualitatively different evolutions for the three motion laws, as well as the different tangential velocities induced by the discrete approximations (2.7a)–(2.7c), (2.6a), (2.6b) and (2.5), (2.4b). In particular, in Fig. 18 one can clearly see that the tangential movement produces approximately uniform meshes throughout, while the evolution in Fig. 17 at times produces quite non-uniform meshes. However, we note that the "ring" structures in the meshes in Figs. 17 and 19 eventually disappear, as can be seen in Fig. 20.

5.5. *Surface diffusion with pinch-off*

In the following, we present an experiment for a "cigar like" rounded cylinder of dimension $8 \times 1 \times 1$ that pinches off under motion by surface diffusion. In order to verify the qualitative features of the evolution as well as to estimate the approximate pinch-off time, i.e. the time when the parametric approximation cannot integrate the solution further due the singularity in the evolution, we used two sets of discretization parameters. For the coarser set we chose $K = 1090$ and $J = 2176$, and used a uniform time step size $\tau = 4 \times 10^{-4}$, while for the finer set of parameters we used $K = 2178$, $J = 4352$, and $\tau = 10^{-4}$. The results can be seen in Figs. 21 and 22, respectively. In Fig. 23 we show plots of the energy decrease and the relative volume loss for each computation. The total relative volume losses for the two computations were −0.15% and −0.03%. We are satisfied that these results agree well. However, it is possible that the later evolution is partly due to numerical effects, as the pinch-off plots differ from what is predicted by asymptotic analysis; see e.g. [9,30]. A detailed investigation of this behaviour will be reported on elsewhere.

The last experiment shows the evolution of a $8 \times 1 \times 1$ cuboid. In order to predict the pinch-off time accurately, we employ the following adaptive time stepping routine. This is necessary because the sharp corners of

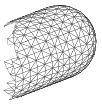

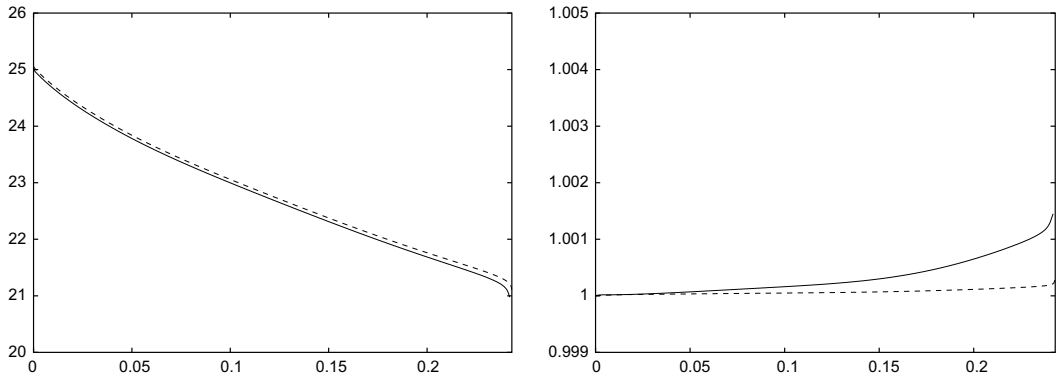

Fig. 23. Plots of the surface area (left) and the relative volume loss (right) for the coarse [solid] and fine [dashed] computation.

the initial parameterization lead to a very fast evolution early on, that can only be captured satisfactory with sufficiently small time steps. To this end, we fix the parameters $\tau_{\min} = 10^{-7}$, $\tau_{\max} \in \{4 \times 10^{-4}, 10^{-4}\}$ and $L = 200$ and use the following algorithm at each time step.

(i) Given $\vec{X}^m$ and τ_m, solve (2.6a), (2.6b) to obtain $\vec{X}^{m+1}$.
(ii) If $\tau_m = \tau_{\min}$, go to (v).
(iii) If $|\Gamma^m| - |\Gamma^{m+1}| > \frac{\delta}{L}$, set $\tau_m := \max\{\frac{\tau_m}{2}, \tau_{\min}\}$ and go to (i).
(iv) If $|\Gamma^m| - |\Gamma^{m+1}| > \frac{\delta}{2L}$, set $\tau_m := \max\{\frac{\tau_m}{2}, \tau_{\min}\}$.
(v) If $|\Gamma^m| - |\Gamma^{m+1}| < \frac{\delta}{10L}$, set $\tau_m := \min\{2\tau_m, \tau_{\max}\}$.
(vi) Set $\tau_{m+1} := \tau_m$ and $m := m + 1$; and go to next time step.

Here $\delta := |\Gamma^0| - 4\pi(\frac{3\mathrm{Vol}(\Gamma^0)}{4\pi})^{\frac{2}{3}}$ is an upper bound for the expected decrease in the surface area. The algorithm above ensures that the surface energy is decreased by at most $\frac{\delta}{L}$ per time step, subject to a minimum time step constraint.

The first experiment uses a parameterization with $K = 1090$ vertices and $J = 2176$ triangles, as well as our adaptive time stepping algorithm with $\tau_{\max} = 4 \times 10^{-4}$. The second experiment uses a parameterization with $K = 2178$ vertices and $J = 4352$ triangles, and uses $\tau_{\max} = 10^{-4}$. The respective results can be seen in Figs. 24 and 25. In Fig. 26 we show plots of the energy decrease and the relative volume loss for each computation. The total relative volume losses for the two computations were -0.12% and -0.01%. We are satisfied that these results agree well with each other.

It is clear that the singular nature of the pinch-off evolution is beyond the capabilities of our direct parametric approximation. As the approximation to the surface is forced to stay connected throughout, the evo-

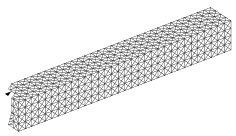

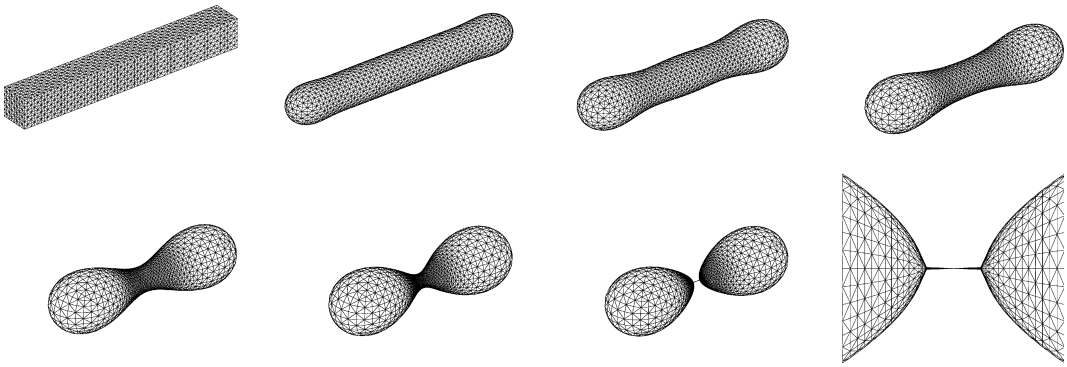

Fig. 25. $\vec{X}(t)$ for $t = 0, 0.01, 0.1, 0.2, 0.3, 0.36, 0.369$. The final plot shows a blowup of the pinch-off at time $t = 0.369$.

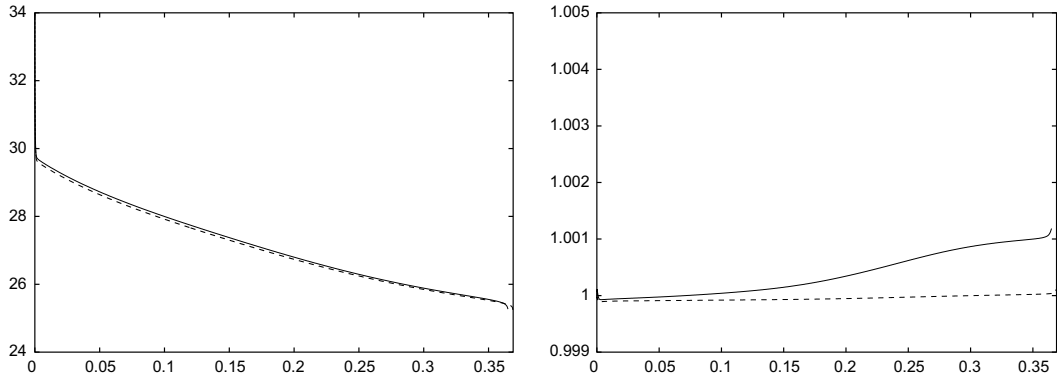

Fig. 26. Plots of the surface area (left) and the relative volume loss (right) for the coarse [solid] and fine [dashed] computation.

lution close to pinch-off in Fig. 25 once again deviates from what the asymptotic analysis predicts. It is therefore probable that the last plots in Figs. 24 and 25 are numerical artifacts. Furthermore, we note that both the approximate pinch-off time as well as qualitative features of our evolution differ from the corresponding results obtained in [4].

6. Conclusions

We have presented a fully practical finite element approximation for the motion by mean curvature and motion by surface diffusion of hypersurfaces in $\mathbb{R}^3$, as well as for other related second and fourth order geometric evolution equations. To our knowledge, for $d = 3$ the proposed algorithms for the nonlinear mean curvature flow (1.4), with e.g. (1.5) and (1.6), and for the intermediate flow (1.9) are the first numerical approximations of these flows in the literature. Moreover, all of the presented schemes intrinsically move the vertices tangentially along the hypersurface, so that no artificial redistribution of vertices is necessary in practice. Finally, we note that extending the presented schemes to more complicated fourth order flows, such as the Willmore flow, as well as generalizing the scheme to incorporate triple junction lines and quadruple junction points between surfaces, and to include anisotropy will be the subjects of our ongoing research in this area. Here we refer to [6,8] for first results in these directions.

References

[1] L. Alvarez, F. Guichard, P.-L. Lions, J.-M. Morel, Axioms and fundamental equations of image processing, Arch. Rational Mech. Anal. 123 (3) (1993) 199–257.

[2] S. Angenent, G. Sapiro, A. Tannenbaum, On the affine heat equation for non-convex curves, J. Amer. Math. Soc. 11 (3) (1998) 601–634.
[3] E. Bänsch, Finite element discretization of the Navier–Stokes equations with a free capillary surface, Numer. Math. 88 (2) (2001) 203–235.
[4] E. Bänsch, P. Morin, R.H. Nochetto, A finite element method for surface diffusion: the parametric case, J. Comput. Phys. 203 (1) (2005) 321–343.
[5] J.W. Barrett, H. Garcke, R. Nürnberg, On the variational approximation of combined second and fourth order geometric evolution equations, SIAM J. Sci. Comput. 29 (3) (2007) 1006–1041.
[6] J.W. Barrett, H. Garcke, R. Nürnberg, Parametric approximation of Willmore flow and related geometric evolution equations, preprint No. 22/2007, University Regensburg, Germany, 2007.
[7] J.W. Barrett, H. Garcke, R. Nürnberg, A parametric finite element method for fourth order geometric evolution equations, J. Comput. Phys. 222 (1) (2007) 441–467.
[8] J.W. Barrett, H. Garcke, R. Nürnberg, A variational formulation of anisotropic geometric evolution equations in higher dimensions, Numer. Math. (2008), in press..
[9] A.J. Bernoff, A.L. Bertozzi, T.P. Witelski, Axisymmetric surface diffusion: dynamics and stability of self-similar pinchoff, J. Statist. Phys. 93 (3–4) (1998) 725–776.
[10] K. Deckelnick, G. Dziuk, C.M. Elliott, Computation of geometric partial differential equations and mean curvature flow, Acta Numer. 14 (2005) 139–232.
[11] M. Desbrun, M. Meyer, P. Alliez, Intrinsic parameterizations of surface meshes, in: G. Drettakis, H.-P. Seidel (Eds.), Eurographics, 2002.
[12] G. Dziuk, An algorithm for evolutionary surfaces, Numer. Math. 58 (6) (1991) 603–611.
[13] G. Dziuk, Convergence of a semi-discrete scheme for the curve shortening flow, Math. Models Methods Appl. Sci. 4 (1994) 589–606.
[14] C.M. Elliott, H. Garcke, Existence results for diffusive surface motion laws, Adv. Math. Sci. Appl. 7 (1997) 465–488.
[15] J. Escher, Y. Giga, K. Ito, On a limiting motion and self-intersections of curves moved by the intermediate surface diffusion flow, Nonlinear Anal. 47 (6) (2001) 3717–3728.
[16] C. Gerhardt, Flow of nonconvex hypersurfaces into spheres, J. Differential Geom. 32 (1) (1990) 299–314.
[17] R. Geroch, Energy extraction, Ann. New York Acad. Sci. 224 (1973) 108–117.
[18] K. Hildebrandt, K. Polthier, M. Wardetzky, On the convergence of metric and geometric properties of polyhedral surfaces, Geom. Dedicata 123 (2006) 89–112.
[19] G. Huisken, T. Ilmanen, The inverse mean curvature flow and the Riemannian Penrose inequality, J. Differential Geom. 59 (3) (2001) 353–437.
[20] P.S. Jang, On the positive energy conjecture, J. Math. Phys. 17 (1) (1976) 141–145.
[21] K. Mikula, D. Ševčovič, Evolution of plane curves driven by a nonlinear function of curvature and anisotropy, SIAM J. Appl. Math. 61 (5) (2001) 1473–1501.
[22] J. Nitsche, Lectures on Minimal Surfaces, Cambridge University Press, Cambrige, 1989.
[23] E. Pasch, Numerische Verfahren zur Berrechnung von Krümmungsflüssen, Ph.D. Thesis, University Tübingen, Tübingen, 1998.
[24] U. Pinkall, K. Polthier, Computing discrete minimal surfaces and their conjugates, Exp. Math. 2 (1) (1993) 15–36.
[25] G. Sapiro, A. Tannenbaum, On affine plane curve evolution, J. Funct. Anal. 119 (1) (1994) 79–120.
[26] A. Schmidt, K.G. Siebert, Design of Adaptive Finite Element Software: The Finite Element Toolbox ALBERTA, Lecture Notes in Computational Science and Engineering, vol. 42, Springer, Verlag, Berlin, 2005.
[27] J. Sullivan, Curvature measures for discrete surfaces, oberwolfach, Preprint. <http://torus.math.uiuc.edu/jms/Papers/>, 2002.
[28] J.E. Taylor, J.W. Cahn, Linking anisotropic sharp and diffuse surface motion laws via gradient flows, J. Statist. Phys. 77 (1994) 183–197.
[29] J.I.E. Urbas, On the expansion of starshaped hypersurfaces by symmetric functions of their principal curvatures, Math. Z. 205 (3) (1990) 355–372.
[30] H. Wong, M.J. Miksis, P.W. Voorhees, S.H. Davis, Universal pinch off of rods by capillarity-driven surface diffusion, Scr. Mater. 39 (1998) 55–60.
[31] G. Xu, Discrete Laplace–Beltrami operators and their convergence, Comput. Aided Geom. Des. 21 (8) (2004) 767–784.